Phonons, phasons, and dislocations in quasicrystals

Joshua E. S. Socolar, T. C. Lubensky, and Paul J. Steinhardt
Department of Physics, University of Pennsylvania, Philadelphia, Pennsylvania 19104
(Received 24 April 1986)

In this paper we examine the detailed relationship between the density-wave and unit-cell descriptions of quasicrystals. We show that phonons, phasons, and dislocations correspond to translations, distortions, and rearrangements of unit cells. The associated density-wave images closely resemble experimental electron micrographs of the icosahedral phase of aluminum-manganese and related alloys. Partial dislocations are also discussed and a natural classification scheme for partials is proposed.

I. INTRODUCTION

The recently discovered icosahedral phase of aluminum-manganese and related alloys[1] may be an example of a new "quasicrystalline" phase of solid matter. Quasicrystals are solids with long-range quasiperiodic translational order and long-range orientational order.[2] Quasicrystals may exhibit any orientational symmetry,[3,4] including those (such as icosahedral symmetry) that are strictly disallowed for periodic crystals. Various techniques have been discussed in the literature for analyzing quasicrystal structure. One approach utilizes a continuum or density-wave description that leads naturally to a Landau theory for quasicrystals. This approach is particularly useful for studying the energetic stability of quasicrystals compared to other ordered states[5–8] and for studying elasticity theory and defects.[6,9,10] A second approach utilizes a discrete or unit-cell picture, describing a quasicrystal as a quasiperiodic packing of two or more unit-cell shapes. This approach is particularly useful for analyzing atomic structure, stoichiometry, diffraction properties, and phonon and electronic wave functions of quasicrystals. Numerous techniques exist for generating quasiperiodic unit-cell packings, including matching and inflation rules,[2,11,12] projections and cuts from higher-dimensional periodic lattices,[4,6,13–15] and the generalized dual (or multigrid) method.[3,13,16]

The purpose of this paper is to discuss the detailed relationship between the density-wave and unit-cell pictures so as to develop a deeper understanding of the structural and elastic properties of quasicrystals:

(i) Landau theory identifies phonon and phason variables whose uniform translations do not change the free energy of the system.[6,9,10] We will show how variations in these variables can be associated with translations, distortions, and rearrangements of unit cells. Locally isomorphic arrangements of unit cells are related by uniform phason shifts (and ordinary translations) and correspond to configurations of equal free energy.

(ii) We produce a series of density-wave images illustrating phonons, phasons, and dislocations which closely resemble experimental electron micrographs of the icosahedral phase of aluminum-manganese and related alloys.[17] The associated unit-cell configurations provide a natural basis for the interpretation of the phonon and phason variables and defects in terms of rearrangements of atoms and atomic clusters.

(iii) We analyze dislocations and partial dislocations in the unit-cell picture. Levine *et al.*[9] have discussed dislocations in the context of the density-wave picture, and Kleman *et al.*[18] have discussed some aspects of dislocations and partials in the unit-cell description. In this paper, we provide a prescription for generating dislocations in the unit-cell picture using either the projection or generalized dual techniques. We also analyze partial dislocations and show how they can be naturally classified as mixtures of two distinct types of partials.

(iv) We discuss the energy and dynamics associated with the phason variable. There appear to be at least two logical possibilities. The first is the elastic-hydrodynamic theory treated in Refs. 9 and 10, which is obtained naturally from the density-wave description. The second, suggested by the tiling picture, is a theory in which excitations occur through local discrete rearrangements[19] leading to defects which can relax through defect diffusion and annihilation.[20] In both cases, phason relaxation is dynamical and controlled by mass diffusion, which is expected to be an extremely slow process in solids.

(v) The correspondence between phasons and rearrangements of unit cells is also relevant to understanding the growth of quasicrystals. One of the arguments that has been raised against the quasicrystal model is that the rapid aggregation of rigid unit cells forced into a quasicrystal structure according to local matching rules (as in a Penrose tiling, say) leads to mismatches.[21] It has been suggested that such mismatches can only be prevented if there are strong long-range interactions (which seems unlikely in an atomic structure). We will see in this paper that the mismatches correspond to spatial variations or strains in the phason variable. We agree that such phason strains will occur during the growth process, and, furthermore, that they will relax slowly (diffusively). However, the energetic cost of such strains is comparable to that of producing strains in periodic crystals and, therefore, should not represent a significant impediment to growth.

The organization of this paper is as follows. In Sec. II, we present a basic overview and discuss the physical significance of our results. In Sec. III, we provide the detailed

mathematical relation between the density-wave and unit-cell constructions. Included is a discussion of how to obtain dislocations in quasicrystals as projections of dislocations in higher-dimensional periodic lattices. In Sec. IV, we discuss how to construct dislocations in unit-cell packings and their associated Burgers vectors. In Sec. V, we extend the methods in Sec. IV to study and classify partial dislocations.

II. PHONONS, PHASONS, AND DISLOCATIONS FROM TWO POINTS OF VIEW

Hydrodynamic modes and topological defects in quasicrystals are most simply described in the density-wave picture, as discussed in Ref. 9. In $(d=2)$-dimensional pentagonal and $(d=3)$-dimensional icosahedral quasicrystals, there are $2d$ broken symmetry hydrodynamic variables, twice as many as in conventional (periodic) crystals. The hydrodynamic modes are the long-wavelength, low-frequency excitations of these variables: d modes can be described as phonon modes and d modes as phason modes associated with the relative displacement of incommensurate density waves. Dislocations correspond to topologically stable spatial variations of combined phonon and phason variables.

The mass density of a periodic solid or quasicrystal can be expanded in a Fourier series of mass density waves with wave numbers drawn from a discrete set of points on a reciprocal lattice. In the Landau density-wave picture of these solid phases, it is customary to include only a finite number of mass density waves in the expansion of the density. Although this approach easily identifies hydrodynamic degrees of freedom, it does not provide detailed information about actual arrangements of atoms or atomic clusters in the solid. The unit-cell picture in both periodic and quasiperiodic solids can provide this information, and so it is useful to interpret variations in the hydrodynamic variables identified with the aid of the Landau theory in terms of translations, distortions, or rearrangements of repeating atomic motifs (unit cells) in quasicrystals. One of the principal goals of this paper is to develop and explore this interpretation.

We begin in this section by briefly reviewing various features of the elasticity and dislocation theory that have been derived from the Landau density-wave description. We then discuss their representation in terms of the unit-cell picture and consider some toy atomic models (decorations of the unit cells) that provide some insight into the nature of the hydrodynamic modes. The mathematical details supporting our assertions in this section are contained in subsequent sections.

For simplicity, we will confine our discussion almost entirely to the two-dimensional tilings with pentagonal orientational symmetry. The generalization to three-dimensional icosahedral structures is straightforward.

A. Review of the Landau density-wave picture

1. Degrees of freedom

To obtain the density-wave description[5,6,9] for an ordered solid, the mass density $\rho(r)$ is expanded in a Fourier series

$$\rho(\mathbf{r})=\sum_{\mathbf{G}\in L_R}\rho_{\mathbf{G}}\exp(i\mathbf{G}\cdot\mathbf{r})\ , \tag{1}$$

where $\mathbf{G}$ is a reciprocal vector and L_R is the reciprocal lattice. Each $\rho_{\mathbf{G}}$ is a complex number with an amplitude $\rho_{\mathbf{G}}$ and a phase $\phi_{\mathbf{G}}$. Since $\rho(\mathbf{r})$ is real, $\rho_{\mathbf{G}}=\rho_{-\mathbf{G}}$ and, hence, $\phi_{\mathbf{G}}=-\phi_{\mathbf{G}}$. The ordered phase can be described in terms of a Landau free energy F that can be expanded in a power series in $\rho(\mathbf{r})$. For example, the kth power of $\rho(\mathbf{r})$ gives rise to terms in F of the form

$$\begin{aligned}F^{(k)}&=A_k\sum_{n1,n2,\ldots,nk}\int d\mathbf{r}\,\rho_{\mathbf{G}_{n1}}\rho_{\mathbf{G}_{n2}}\cdots\rho_{\mathbf{G}_{nk}}\exp\left[\sum_{i=1}^{k}\mathbf{G}_{ni}\cdot\mathbf{r}\right]\\&=VA_k\sum_{\mathbf{G}_n\in L_R}\Delta\left[\sum_{n=1}^{k}\mathbf{G}_n\right]\cos\left[\sum_{n=1}^{k}\phi_{\mathbf{G}_n}\right]\prod_{n=1}^{k}|\rho_{\mathbf{G}_n}|\ ,\end{aligned} \tag{2}$$

where V is the volume. The factor $\Delta(x)\equiv\delta_{x,0}$ ensures that only terms where $\sum_{n=1}^{k}\mathbf{G}_n=0$ contribute to the sum in Eq. (2). The free energy expansion is phenomenological in the sense that the coefficients A_k depend upon the details of the physical system (atomic species, interatomic interactions, temperature, pressure, etc.). The equilibrium ordered state is characterized by the values of $\rho_{\mathbf{G}}$ that minimize F.

The goal of the density-wave description is to derive certain general properties of the ordered state that depend upon the symmetries and conservation laws, but not on the particular choices of A_k. For these purposes, it is sufficient to consider a small finite subset $\{\rho_{\mathbf{G}_n}\}$ of the Fourier components $\rho_{\mathbf{G}}$. In practice, the "density-wave picture" consists of retaining only the set $\{\rho_{\mathbf{G}_n}\}$ in the Fourier expansion of $\rho(\mathbf{r})$ and truncating F at some low power in an expansion in $\{\rho_{\mathbf{G}_n}\}$.

The $\{\rho_{\mathbf{G}_n}\}$ must include a minimal subset of the $\rho_{\mathbf{G}}$ corresponding to N_R reciprocal vectors $\mathbf{G}_n$, such that any reciprocal vector $\mathbf{G}\in L_R$ can be written as an integral linear combination of the $\mathbf{G}_n$. In addition, $\{\rho_{\mathbf{G}_n}\}$ must include reflected images $\{\rho_{-\mathbf{G}_n}\}$ (to ensure a real mass density when all density waves are summed) plus any vectors that can be obtained from the minimal set by point group operations associated with the orientational symmetry of the solid. In periodic crystals, $N_R=d$; in quasicrystals, $N_R=n_i d$, where n_i is the number of incommensurate lengths associated with each lattice vector direction. For pentagonal and icosahedral quasicrystals $n_i=2$. (For icosahedral quasicrystals, the minimal set $\{\rho_{\mathbf{G}}\}$ can be chosen to correspond to the six independent vectors pointing to the vertices of an icosahedron plus reflected images.) For pentagonal quasicrystals, a natural choice for $\{\rho_{\mathbf{G}_n}\}$ consists of the five $\rho_{\mathbf{G}_n}$ corresponding to the five vectors that point to the vertices of a pentagon (plus reflected images): four vectors are required because $n_i d=4$, and a fifth is added because it is related by a point symmetry operation to the other four. The five vectors can be written $G_n=G[\cos(2\pi n/5),\sin(2\pi n/5)]$, $n=0,\ldots,4$. [Later, to discuss partial dislocations, we shall find it use-

ful to extend $\{\rho_{G_n}\}$ to include more reciprocal-lattice vectors (see Sec. V).] Note that, since $\sum_{n=0}^{4} \mathbf{G}_n = 0$, only four of the $\mathbf{G}_n$ are independent.

Minimization of F with respect to $|\rho_{\mathbf{G}}|$ and $\phi_{\mathbf{G}}$ fixes all the variables except for N_R phases. From Eq. (2) it is clear that for any set of $\mathbf{G}_n$'s that satisfies $\sum \mathbf{G}_n = 0$, the value of F depends on the value of $\sum \phi_{G_n}$. Minimizing F must, therefore, fix the value of every such sum. For the pentagonal case then, where our chosen fundamental set of five $\mathbf{G}_n$'s satisfies $\sum \mathbf{G}_n = 0$, minimizing F places the constraint that $\sum \phi_{G_n} = \Gamma = \text{const}$, and only $N_R = 4$ phases remain independent.

Because uniform shifts in the N_R phases leave F unchanged, they correspond to hydrodynamic variables in the theory. Furthermore, *uniform shifts in the ϕ_{G_n} that change the sum of the phases change the energy.* (Such a uniform shift corresponds to a shift in local isomorphism class in the unit-cell picture.) The $N_R = 4$ hydrodynamic degrees of freedom in phases can be parametrized by two two-dimensional vectors, $\mathbf{u}$ and $\mathbf{w}$, which are related to two different vector representations of the rotational symmetry group. For pentagonal symmetry, a convenient parametrization is[9]

$$\phi_{G_n} = \mathbf{u}\cdot\mathbf{G}_n + a\,\mathbf{w}\cdot\mathbf{G}_{\langle 3n\rangle} + \Gamma/5, \quad n = 0, \ldots, 4 , \qquad (3)$$

where $\langle 3n \rangle$ means $\mathrm{mod}_5(3n)$ and $a = \sin(2\pi/5)/\sin(4\pi/5)$. In the perfectly ordered state $\mathbf{u}$ and $\mathbf{w}$ are constant vector fields (independent of position). Figure 1(a) depicts such a "density-wave image" obtained by computing the truncated $\rho(\mathbf{r})$,

$$\rho(\mathbf{r}) = \sum_{\alpha=0}^{4} \cos(\mathbf{G}_n\cdot\mathbf{r} + \phi_{G_n}) ,$$

where $\sum \phi_{G_n} = 0$, in the manner described in Ref. 9. These and other density-wave images shown in this paper are different from those in Ref. 9 in that they are, in some sense, "higher contrast" and black and white are reversed. White dots indicate regions where $\rho(\mathbf{r})$ is positive and at least $\frac{2}{5}$ of the maximum possible positive value of $\rho(\mathbf{r})$ [whereas in Ref. 9 white dots meant only that $\rho(\mathbf{r}) < 0$]. This cutoff is essentially arbitrary, but we have made the choice of $\frac{2}{5}$ here because it produces images that compare better visually with experimental electron micrographs. Note how the white dots lie along quasiperiodically spaced parallel lines oriented parallel to edges of a pentagon. In Fig. 2(a), a similar figure except with $\sum \phi_{G_n} = 0.3$ is shown. Figures 1(a) and 2(a) correspond to density-wave images associated with two states with differing free energy. They correspond to the density-wave images expected for unit-cell configurations in different local isomorphism classes.

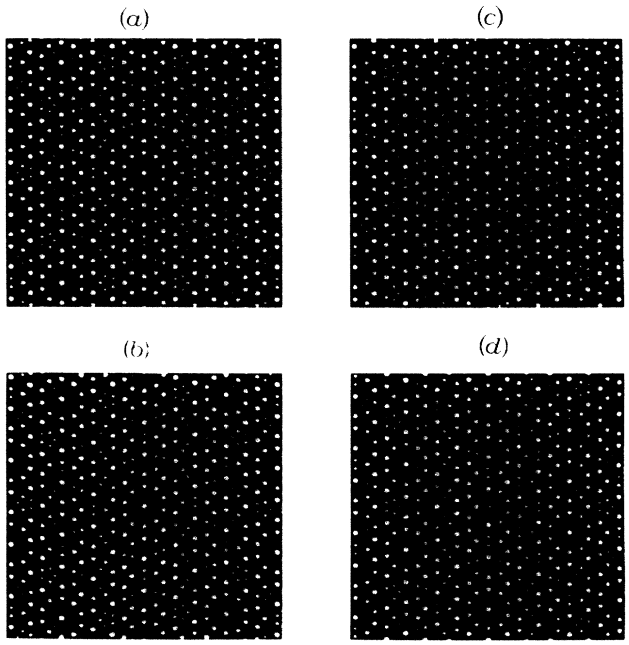

FIG. 1. Density-wave images. A white dot is placed at all points $\mathbf{r}$ where the value of $\rho(\mathbf{r})$ exceeds $\frac{2}{5}$ of its maximum value. (a) A perfect pattern with $\sum \phi_{G_n} = 0$. (b) A distortion of pattern (a) corresponding to spatial variations in the phonon degree of freedom $\mathbf{u}$. (c) A pattern containing variations in the phason degree of freedom $\mathbf{w}$ about the value used in pattern (a). (d) A dislocation. Note that both phonon variations (curvature) and phason variations (jags) are present.

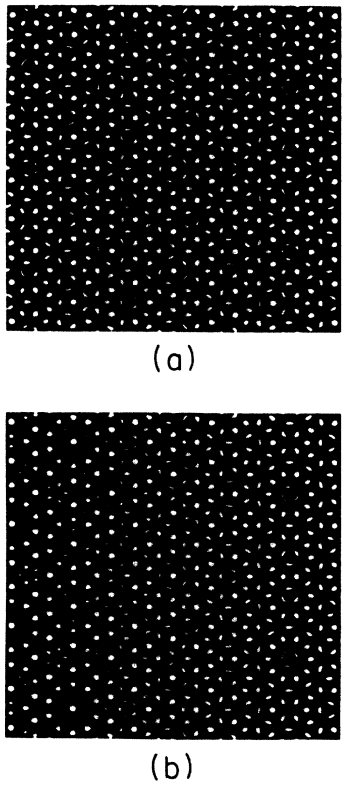

FIG. 2. Density-wave images. (a) A perfect pattern with $\sum \phi_{G_n} = 0.3$. (b) A pattern in which $\sum \phi_{G_n}$ varies linearly from zero on the left to 0.5 on the right. Variations in $\sum \phi_{G_n}$ correspond to variations in local isomorphism class in the unit-cell picture.

2. *Variations in* $\mathbf{u}$

A uniform shift in $\mathbf{u}$ corresponds to a translation of the system. Just as in the case of a periodic crystal, spatial

variations in **u** give rise to propagating phonons. Figure 1(b) is a density-wave image with constant **w** but varying **u**. Note the curvature produced in the lines of high-density points.

3. *Variations in* **w**

A uniform change in **w** shifts the density waves relative to one another to produce a rather subtle change in the pattern. Mathematically, the **w** variable is analogous to the phason degree of freedom in incommensurate crystals. One of our primary concerns will be to interpret uniform shifts in **w** in terms of special rearrangements of the unit cells.

Figure 1(c) shows a density-wave image with constant **u** and varying **w**. In contrast to Fig. 1(b) in which only **u** is varied, the high-density regions remain along straight lines, but the lines are jagged or shifted in many places. Interestingly, some experimental electron micrographs of icosahedral phases exhibit shifts similar to those that we find for phason variations.[17] This observation is consistent with the hydrodynamic theory which suggests that phason variations present when a sample is prepared take a very long time to relax.[10]

Figure 2(b) shows a density-wave image in which $\sum \phi_{\mathbf{G}_n}$ varies from zero on the left-hand side to 0.5 on the right-hand side of the image. Such an image corresponds to a variation in local isomorphism class. According to the hydrodynamic theory, such variations are highly energetic excitations that should relax quickly to the ground state. This is consistent with the fact that we have not observed such variations in experimental electron micrographs.

Note that the method of obtaining electron micrograph images—Fourier transforming some subset of diffraction spots lying in a two-dimensional (2D) plane—is exactly equivalent to the way in which we have obtained our 2D density-wave images. Therefore, it is appropriate to compare directly the 2D density-wave images in this paper with electron micrographs obtained by imaging fivefold diffraction patterns of icosahedral phases.

4. *Dislocations*

Dislocations are topologically stable point defects in two dimensions or line defects in three dimensions corresponding to spatial variations in the phases, $\phi_{\mathbf{G}_n}$, or, equivalently, the vector fields **u** and **w**. They are characterized by a Burgers vector which measures the net displacement in **u** and **w** (with respect to a perfect lattice) about any circuit enclosing the dislocation core. The Burgers vector can be expressed as a $2d$ dimensional vector, the first d components of which measure the displacement in **u** and the second d components of which measure the displacement in **w**.[9]

The Burgers vectors correspond to displacements in **u** and **w** that leave the $\phi_{\mathbf{G}_n}$ invariant modulo 2π (and keep the sum of the phases fixed for the case of pentagonal symmetry). As shown in Ref. 9, each Burgers vector corresponds to nonzero **u** (translational) and **w** (phason) displacements, so that dislocations in quasicrystals, unlike those in periodic crystals, cannot be interpreted simply in terms of insertions or removals of half-planes of atoms (pure translations).

Figure 1(d) illustrates a density-wave image of a dislocation whose core lies at the origin. We have set $\phi_{\mathbf{G}_1}=-\phi_{\mathbf{G}_4}=\theta$ (keeping $\sum \phi_{\mathbf{G}_n}$ fixed), where θ is the usual polar angle. The dislocation contains both curvature and jags, indicating that variations in both **u** and **w** are present. For these images, the variation in the phases has been chosen to be circularly symmetric (proportional to θ), so that the curvature and jags are distributed in a circularly symmetric pattern. However, in real materials, a phase variation which is not uniform in θ may be energetically favorable.[22]

B. Unit-cell picture

In the unit-cell description of a quasicrystal, specifying the orientational symmetry and the shapes of the unit cells is not sufficient to uniquely determine the tiling (packing of unit cells).[23] In fact, there are infinitely many distinguishable rearrangements of the unit cells whose diffraction patterns are given by the same set of reciprocal wave vectors with different Bragg peak intensities. The tilings can be subdivided into *local isomorphism* (LI) classes, where two tilings are in the same LI class if, and only if, every bounded configuration of unit cells in each is found in the other. The condition that two tilings be in the same LI class guarantees that the tilings cannot be distinguished by measurements made on any finite length scale. Tilings in the same LI class are, therefore, physically indistinguishable and have identical Fourier transform (diffraction) properties *including intensities.* The phases are also identical up to shifts which preserve the value of $\sum \phi_{\mathbf{G}_n}$ for every set $\{\mathbf{G}_n\}$ that satisfies $\sum \mathbf{G}_n=0$. A physical consequence is that configurations in the same LI class have the same free energy density F, since F just depends on the Fourier coefficients; conversely, tilings in different LI classes will have different free energies, unless there is some accidental energy degeneracy. In particular, if we are interested in analyzing an atomic structure in terms of unit cells, we should focus on the subset of tilings belonging to the LI class with minimum F.[23]

1. *Degrees of freedom and local isomorphism*

As we shall detail in Sec. III, associated with each of the techniques for constructing quasicrystal unit-cell packings are parameters analogous to $|\rho_{\mathbf{G}}|$ and $\phi_{\mathbf{G}}$ in the density-wave description. For example, some of these parameters control the precise position of the five-dimensional (5D) lattice points (or, equivalently, of the projection strip) in the projection approach and the relative shifts of the grids of parallel lines in the generalized dual approach. Just as minimizing F determines all the $|\rho_{\mathbf{G}}|$ and $\phi_{\mathbf{G}}$ except for N_R phases in the density-wave picture, so fixing the LI class determines all but N_R of the parameters in the unit-cell picture. The N_R parameters can be expressed in terms of two vectors, $\mathbf{u}_t$ and $\mathbf{w}_t$, analogous to **u** and **w** in the density-wave picture. The

vector $\mathbf{w}_t$ determines the particular unit-cell configuration within the LI class and $\mathbf{u}_t$ determines the translation of the pattern.

The tilings produced by Penrose by application of matching and inflation rules[11] correspond to a particular subset—a single LI class—of pentagonal quasicrystal tilings. Without loss of generality, we will focus on this particular LI class to illustrate our points, as if the Penrose LI class corresponded to the ground state of some system. This LI class has the advantage that many readers are already familiar with Penrose tilings. Distortions and defects in these tilings are easy to recognize and their energetics can be estimated in terms of violations of the matching conditions. Furthermore, the Penrose LI class has the advantage that it can be generated as a simple decoration of an "Ammann quasilattice"[24] of quasiperiodically spaced parallel lines. The effect on the lines in the Ammann quasilattice induced by distortion and defects in the unit-cell structure bears a remarkably close resemblance to the analogous effects on the lines of high-density points (black dots) in the density-wave images.

For fixed LI class, the perfectly ordered tiling correspond to spatially uniform $\mathbf{u}_t$ and $\mathbf{w}_t$. In Fig. 3(a) we illustrate a portion of a perfectly ordered Penrose tiling. [See also Fig. 4(a), which is explained in Sec. III.]

2. *Variations in* $\mathbf{u}_t$

Uniform shifts in $\mathbf{u}_t$ give rise to pure translations of a Penrose tiling. Spatial variations in $\mathbf{u}_t$ lead to distortions of the tile shapes but do not affect the configuration of tiles at any point. This corresponds precisely to the situation in periodic crystals where spatial variations of the phonon field can be thought of as distortions of the unit cells. Thus the correspondence between $\mathbf{u}$ of the Landau theory and $\mathbf{u}_t$ is simple and direct. Figure 3(b) illustrates a Penrose tiling with spatially varying $\mathbf{u}_t$. [See also Fig. 4(b).]

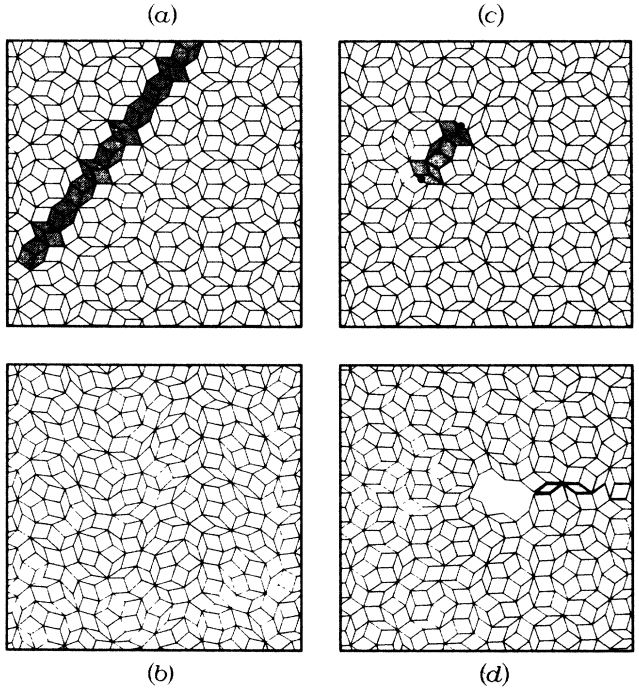

FIG. 3. Penrose tilings. (a) A portion of a perfect Penrose tiling. The shaded unit cells compose a segment of a "worm." (b) A distortion of the tiling of (a) corresponding to variations in the phonon degree of freedom $\mathbf{u}_t$. The unit-cell shapes are distorted, but their arrangement is the same as in (a). (c) A tiling containing variations in the phason degree of freedom $\mathbf{w}_t$ about the value used in (a). The shaded rhombuses form a flipped segment of a worm. [Compare to same region of (a). For more details on worm flips, see Fig. 5.] The large dots at the ends of the shaded segment indicate edges along which the Penrose matching rules are violated—deviations from the Penrose local isomorphism class. This picture contains several other such mismatches and flipped worm segments. To find them, use Fig. 4 as a guide. (d) A dislocation in a Penrose tiling. At large distances from the core the distortion of the unit cells and the density of mismatches both become small, although neither can be completely eliminated.

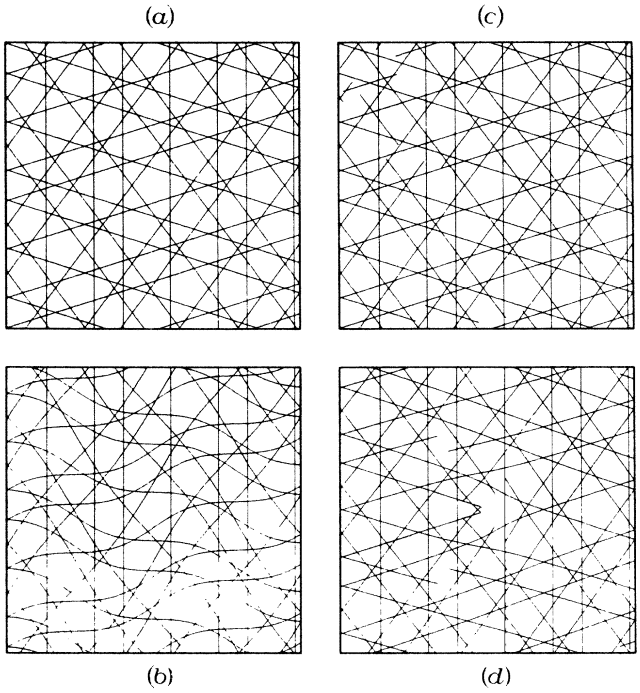

FIG. 4. Ammann quasilattices. A Penrose tiling can be obtained from an Ammann quasilattice either by decoration or by a generalized dual transformation. The reader is encouraged to overlay a transparency of this figure on Fig. 3. (a) A portion of a perfect Ammann quasilattice corresponding to the Penrose tiling of Fig. 3(a). (b) A distortion of the Ammann quasilattice of (a) corresponding to variations in the phonon degree of freedom $\mathbf{u}_t$. (c) An Ammann quasilattice containing variations in the phason degree of freedom $\mathbf{w}_t$ about the value used in (a). The points at which a line shifts, called "jags," correspond precisely to mismatches in the associated tiling. [Compare to same region of Fig. 3(c).] (d) A dislocation in an Ammann quasilattice. At large distances from the core the curvature of the lines and the density of jags both fall off like $1/r$.

3. *Variations in* $\mathbf{w}_t$

Uniform shifts in $\mathbf{w}_t$ produce no tile distortion or uniform translation but, instead, result in special rearrangements of the tiles which transform the tiling to another tiling within the same LI class.

The rearrangements induced by uniform shifts in $\mathbf{w}_t$ can be understood as taking place along so-called "worms" in the tiling. A "worm" is composed of thick and thin rhombuses which form a connected line of (irregular) hexagons, as shaded in Fig. 3(a). If the hexagons formed from one thin and two thick rhombuses are labeled S and the hexagons formed from one thin and two thick rhombuses are labeled F, then the worm is given by a Fibonacci sequence of S and F hexagons. Each tiling contains an infinite number of crisscrossing worms. In most worms, the worm of hexagons is interrupted in several places due to the crossing of some other worm. An entire uninterrupted worm is unique in that it can be reflected about its horizontal axis, or "flipped," without disrupting any of the Penrose matching rules (or, equivalently, without changing the LI class). When a hexagon consisting of two thin tiles on top and one thick tile on the bottom, say, is flipped, the tiles are rearranged within the same hexagonal boundary such that the thick tile is now at the top and the matching rules in the interior of the hexagon are still obeyed. (See the transformation in the rightmost hexagons in the two lower diagrams of Fig. 5.) A flipped worm is obtained by flipping all of its constituent hexagons.

In general, a uniform shift in $\mathbf{w}_t$ causes a number of crisscrossing worms to flip in just such a way that the matching rules are maintained throughout (including where the two worms cross). The number density of worms that flip is proportional to the size of the change in $\mathbf{w}_t$. In the Penrose tilings, spatial variations in $\mathbf{w}_t$ result in segments of worms being flipped, creating isolated violations of the matching rules. The matching rule violation occurs only at the two ends of the segment, along the two hexagon edges that connect to the rest of the worm. In other words, the flip leads to two localized defects at the ends of the worm segment. Examples of such mismatches are indicated in Fig. 3(c), which shows the result of varying $\mathbf{w}_t$ on a Penrose tiling. [See also Fig. 4(c).] We note that in the analogous three-dimensional structures, a "worm" consists of a planar array of connected unit cells. Spatial variations in $\mathbf{w}_t$ lead to flipping of the unit cells in connected planar sections of a worm producing lines of mismatches along the boundaries of the sections. For a brief explanation of this result, see Sec. III A.

Note that such mismatches will occur naturally during the rapid aggregation of unit cells during quasicrystal growth. That is, given only local interactions or matching rules that lead to a ground state corresponding to some particular LI class, mismatches can be produced where a worm of unit cells growing in one direction meets a flipped worm growing from the opposite direction. It has even been suggested that mismatches might represent a significant impediment to the growth of quasicrystals (unless there are strong long-range interactions to prevent them).[21] We now see that such mismatches correspond to

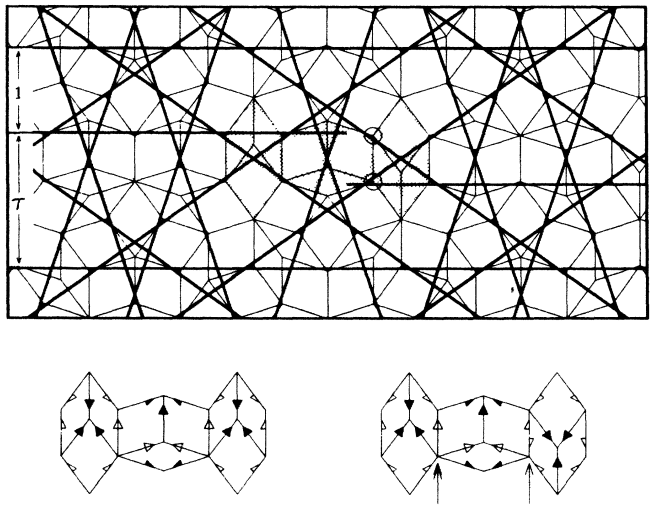

FIG. 5. Illustration of a "worm" in a Penrose tiling and its signature in the Ammann quasilattice. An open circle indicates a type of vertex that is never found in undefected tilings of the Penrose local isomorphism class. The right (left) half of the broken Ammann line can be shifted up (down) to restore the ideal quasilattice in the region depicted. The consequent rearrangements of the intersections of the Ammann quasilattice cause the right (left) half of the worm to flip when the generalized dual technique is applied. The worm segments depicted below are decorated to illustrate the Penrose matching rules. The rules are that two tiles can join only along edges which have the same color arrow pointing in the same direction. The segment on the right corresponds to the shaded segment above, where the rightmost hexagon (formed from one thick and two thin rhombuses) has been flipped, causing a matching rule violation (indicated by the single arrow). If the middle hexagon were now flipped to relieve that mismatch, a mismatch would arise along the edge indicated by the double arrow. Note, however, that the top and bottom of the hexagon are decorated in the same way, so that no other mismatches would arise.

spatial variations or strains in the phason variable which can relax in a diffusive mode through local rearrangements of atoms. (During rapid cooling, there may also be local deviations from the ground-state LI class, but we expect these to relax quickly because they are energetically costly according to the Landau theory.) Of course, dislocations and compositional variations may be quenched during rapid solidification since they also relax slowly.

The detailed way in which a phason relaxes depends to some degree on the appropriate model of the dynamics. Considering the tiles themselves for a moment, we see that a mismatch can be moved along the worm that contains it by successive flips of single hexagons. A worm that contains mismatches can therefore relax to the ground state by having those mismatches find each other and annihilate or move off to infinity. Figure 6 shows a sequence of configurations corresponding to the relaxation of a localized "bump" in the $\mathbf{w}_t$ field. (See also Fig. 7.)

4. *Dislocations*

In the unit-cell description of a quasicrystal, a dislocation produces a topologically stable rearrangment and dis-

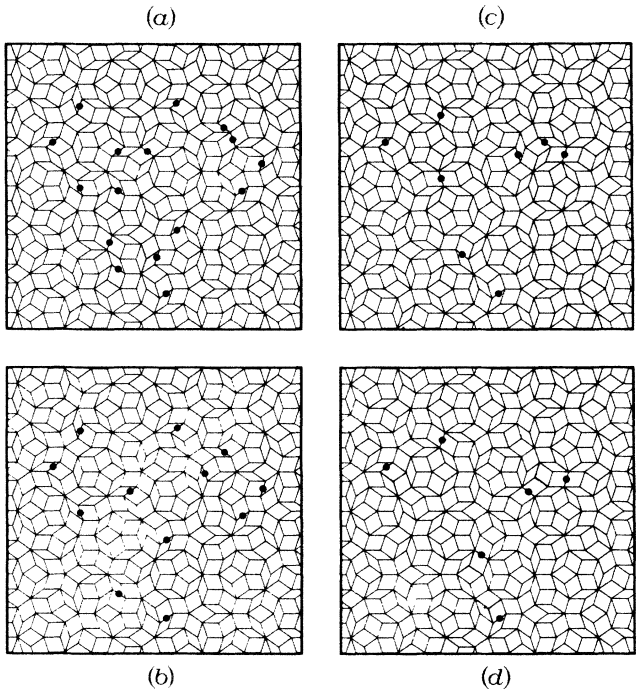

FIG. 6. Tiling illustration of the relaxation of a localized variation ("bump") in the phason field. In each figure we have set $\mathbf{w}_t = A(r)\hat{\mathbf{y}}$, where $A(r) = A_0[1+\cos(kr)]$ for $kr < \pi$ and $A(r) = 0$ at greater values of r. The value of k is such that $kr = 2\pi$ occurs near the border of the figure; there are no variations in $\mathbf{w}_t$ that are not visible. The value of A_0 decreases steadily through the sequence (a), (b), (c), (d). Dots indicate mismatches in the tiling (deviations from the Penrose LI class). Note that the order in which the mismatches annihilate is not arbitrary. Some worms cannot flip until other crossing worms do.

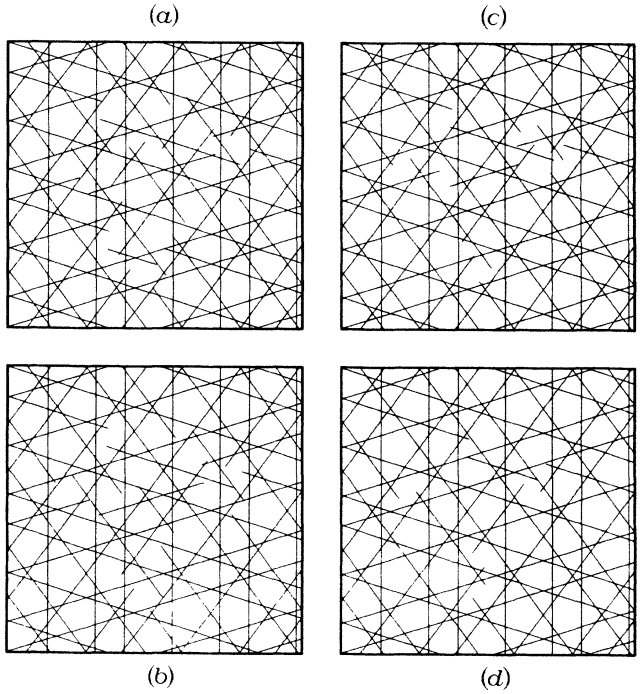

FIG. 7. Ammann quasilattice illustration of the relaxation of a bump in the phason field. In each figure we have set $\mathbf{w}_t = A(r)\hat{\mathbf{y}}$, where $A(r) = A_0[1+\cos(kr)]$ for $kr < \pi$ and $A(r) = 0$ at greater values of r. The value of k is such that $kr = 2\pi$ occurs near the border of the figure; there are no variations in $\mathbf{w}_t$ that are not visible. The value of A_0 decreases steadily through the sequence (a), (b), (c), (d). These pictures can be compared directly to those of Fig. 6. Note that each mismatch in the tiling corresponds to a jag in the Ammann quasilattice.

tortion of the unit cells. The dislocation can be characterized by the net displacement in $\mathbf{u}_t$ and $\mathbf{w}_t$ with respect to the undefected unit-cell structure as measured around a closed path that encircles the dislocation core (a Burgers circuit). Because the dislocation is a topological point defect in two dimensions (2D) (or line defect in 3D), as the radius of the Burgers circuit about the core approaches infinity, the local arrangements and shapes of the unit cells along the circuit become indistinguishable from those in the undefected lattice (i.e., the same unit-cell shapes and the same LI class).

From these simple remarks, we can understand why any dislocation in the quasicrystal tiling requires displacements in *both* $\mathbf{u}_t$ and $\mathbf{w}_t$. If a defect involved only displacements in the translational degree of freedom, $\Delta\mathbf{u}_t = \mathbf{b}$, the tiling arrangement could not approach the LI class of the undefected lattice at large distances from the dislocation core. The tiles at the beginning and end of a large Burgers circuit would not match in an arrangement in the same LI class unless $\mathbf{b}$ were an exact translation vector of the lattice; however, there is no such translation vector in a quasiperiodic structure. To approach the LI class of the undefected tiling at large distances from the core, as required for a dislocation, the translation $\Delta\mathbf{u}_t$ must be accompanied by a rearrangement of unit cells, as occurs through displacement in the phason variable $\mathbf{w}_t$.

To form a dislocation in a Penrose tiling we make $\mathbf{u}_t$ and $\mathbf{w}_t$ functions of the polar angle θ, as measured about the dislocation core. The requirement that there be no mismatches along the $\theta = 0$ ray (to require matching at the beginning and end of a Burgers circuit) forces a certain relationship between $\Delta\mathbf{u}_t = \mathbf{u}_t(2\pi) - \mathbf{u}_t(0)$ and $\Delta\mathbf{w}_t = \mathbf{w}_t(2\pi) - \mathbf{w}_t(0)$, as we will demonstrate in the next section. The dislocation can then be characterized by a $2d$-dimensional vector, the first two components of which measure the displacement in $\mathbf{u}_t$ and the second two components of which measure the displacement in $\mathbf{w}_t$. The properties of this vector and the constraints on it are exactly the same as those found for the Burgers vectors in the Landau theory. Thus, we will refer to this vector as the Burgers vector when discussing the unit-cell picture. Note that in a dislocation, $\mathbf{u}_t$ and $\mathbf{w}_t$ are interlocked and neither can relax to a constant. A dislocation in a Penrose tiling is shown in Fig. 3(d). [See also Fig. 4(d).]

One advantage of the unit-cell picture over the five-component density-wave picture is that it leads to a more complete understanding of dislocations and partial dislocations. According to the simple Landau theory, for example, topological defects need be introduced in only two of the five phases in order to form a dislocation. One

might therefore expect that a dislocation in a tiling could be formed in which mismatches occurred only along worms running in two of the five possible directions. The density-wave picture of Fig. 1(d) shows, however, that jags occur along four directions and Fig. 3(d) shows that mismatches in the tiling also occur along four directions.

The disparity is due to the effect induced on the phases of other $\rho_{\mathbf{G}}$ when the fundamental $\phi_{\mathbf{G}_n}$'s are changed. Whereas the simple Landau density-wave theory includes only the fundamental $\rho_{\mathbf{G}_n}$, the unit-cell picture automatically includes other $\rho_{\mathbf{G}}$ (higher harmonics). (The method of obtaining the density-wave image from a sum of cosine waves also introduces higher harmonics, as can be seen by diffracting a laser from one of the density-wave images.) The defect can be understood from the density-wave picture if we expand $\{\rho_{\mathbf{G}_n}\}$ to include five more $\rho_{\mathbf{G}}$ corresponding to the wave vectors $\mathbf{G}'_n=(1/\tau)\mathbf{G}_n$ (plus reflected images). (No extra hydrodynamic variables are introduced by this construction.) Note that $\mathbf{G}'_n-\mathbf{G}_{n-1}-G_{n+1}=0$, implying that $\phi_{\mathbf{G}'_n}-\phi_{\mathbf{G}_{n-1}}-\phi_{\mathbf{G}_{n+1}}=\text{const}$, where the constant is determined by minimizing F. Thus, if we set, for example,

$$\phi_{\mathbf{G}_1}=-\phi_{\mathbf{G}_4}=f(x,y),\quad \phi_{\mathbf{G}_0}=\phi_{\mathbf{G}_2}=\phi_{\mathbf{G}_3}=\text{const}\ ,$$

the constraints on the sums of the phases require that

$$\phi_{\mathbf{G}'_2}=-\phi_{\mathbf{G}'_3}=f(x,y)+\text{const}\ ,$$

$$\phi_{\mathbf{G}'_0}=\phi_{\mathbf{G}'_1}=\phi_{\mathbf{G}'_4}=\text{const}.$$

The variations in $\phi_{\mathbf{G}_1}$ and $\phi_{\mathbf{G}_4}$ cause mismatches in the $\mathbf{G}_1$ and $\mathbf{G}_4$ directions as expected, but they also induce variations in $\phi_{\mathbf{G}'_2}$ and $\phi_{\mathbf{G}'_3}$, which accounts for the mismatches found in the $\mathbf{G}_2$ and $\mathbf{G}_3$ directions. We further consider topologically stable variations in these extra phases in our analysis of partial dislocations, as discussed in Sec. IV.

C. Energy and dynamics of u and w spatial variations and dislocations

In the Secs. II A and II B, we discussed the effects of spatial variations of $\mathbf{u}$ and $\mathbf{w}$ on the structure of pentagonal quasicrystals using both the density-wave and unit-cell pictures. It was not necessary in this discussion to make any reference to energies associated with these variations. In real physical systems, however, the energetics associated with spatially varying hydrodynamic variables is of considerable interest. In this section, we will discuss two logical possibilities for the energetics.

In the standard elastic picture, $\mathbf{u}$ and $\mathbf{w}$ are regarded as continuum hydrodynamic variables having an elastic energy proportional to the square of their gradients. This is the approach discussed in Refs. 6, 9, and 10. A change, $\Delta\mathbf{w}$, in $\mathbf{w}$ along a single direction in a d-dimensional cube of side L gives rise to an elastic energy of order $\approx L^{d-2}(\Delta\mathbf{w})^2$, since the change in $\mathbf{w}$ is distributed uniformly along L ($\nabla\mathbf{w}\approx\Delta\mathbf{w}/L$), just like the energy associated with a Bloch wall in a Heisenberg ferromagnet. In a dislocation, $\nabla\mathbf{w}\propto r^{-1}$, where r is the distance from the core. The elastic energy of a dislocation in a two-dimensional sample is, thus, of order $\ln(L/a)$, where a is the core radius. The hydrodynamics implied by this continuum elastic picture (and the symmetries and conservation laws of the icosahedral phase) is discussed in Ref. 10. The dynamic modes associated with $\mathbf{u}$ are propagating phonons, whereas those associated with $\mathbf{w}$ are diffusive. Note that the relaxation of the spatial variations in the phason variable in Fig. 6 occurs through local rearrangements of unit cells and is perfectly consistent with the hydrodynamic theory which predicts relaxation through local diffusive motion of atoms.

In an alternate approach, which is suggested by the unit-cell picture, spatial variations in $\mathbf{u}$ lead to distortions in unit-cell sizes and shapes. Since unit cells can be continuously distorted, it is natural to associate an elastic energy with spatial variations in $\mathbf{u}$, just as for a periodic solid. Spatial variations in $\mathbf{w}$, on the other hand, give rise to matching rule violations at discrete places in the lattice. A violation is either present or it is not, and the natural way to determine the energy of a spatial variation in $\mathbf{w}$ would be to associate an energy ϵ with each matching rule violation. The energy E associated with a given configuration with nonuniform $\mathbf{w}$ is then $E=N_m\epsilon$, where N_m is the number of matching rule violations. Along a given line, the number of matching rule violations is proportional to $|\Delta\mathbf{w}|$, so that $E\approx L^{d-1}|\Delta\mathbf{w}|\approx L^d|\nabla\mathbf{w}|$. The energy of a dislocation is then proportional to $\int d^2r\,|\nabla\mathbf{w}|\approx L$.

Note that the energy associated with a slowly varying $\mathbf{w}$ still goes to zero (linearly) with wave number (in the limit of long wavelength). Thus $\mathbf{w}$ remains distinguished from variables such as those corresponding to variations in LI class which are nonhydrodynamic in the density-wave picture. Spatially uniform shifts (i.e., the limit of long-wavelength variations) of the latter produce energy increases proportional to the volume of the sample.

The dynamics of the discrete model suggested by the unit-cell picture is not yet fully understood. The Frenkel-Kontorova model[25] is one of the simplest models for incommensurate structures and may provide insight concerning this topic. It consists of a linear chain of atoms coupled by ideal (Hooke's law) springs of equilibrium length l_0 interacting with a rigid "washboard" giving rise to a cosine potential of incommensurate period l_1. The energy is invariant with respect to uniform translations of the chain atoms relative to the washboard. When the average separation of the atoms is constrained to be an irrational multiple of the washboard period, there is an elastic phason energy proportional to the square of the gradient of the atomic variable so long as the washboard potential is not too strong. However, for sufficiently strong washboard potential, numerical calculations by Peyrard and Aubry[26] show that the position of the nth atom becomes a discontinuous function of n and the energy associated with very slow spatial variations of position becomes finite rather than infinitesimal.[26] That is, the energy becomes Ising-like rather than elastic. Peyrard and Aubry refer to the state with discontinuous position variable as *pinned* since neighboring states of equivalent energy are separated by an energy barrier.

One could argue that the unit-cell description, a discrete

picture in which spatial variations in the phason variable correspond to discrete rearrangements of the unit cells which produce mismatches, is naturally associated with the pinned state.[19] If this is the case, continuum elasticity[9] and hydrodynamics[10] is not applicable. Nevertheless, it appears that phason relaxation can occur through diffusion and annihilation of defects. Thus, even though the detailed energetics and dynamics may be different from the hydrodynamic results, long-wavelength phason strain is a low-energy excitation and long-wavelength phason relaxation is a slow, diffusive process that plays an important role in the elastic properties of quasicrystals.[20]

We wish to emphasize that even if the elasticity is correctly described by the continuum approach, it can also be interpreted in terms of a unit-cell picture. We adopt the point of view that the unit cells provide a template for local atomic configurations, but do not determine the dynamics. Within each unit cell in an equilibrium configuration, there is a preferred arrangement of atoms, which depends upon the unit-cell shape and the matching rules (or, more generally, LI class). Other atomic arrangements are energetically unfavorable. A matching rule violation, which is produced by a local rearrangement of unit cells, can be interpreted as an energetically unfavorable rearrangement of atoms. Such a rearrangement of atoms will cause the positions of atoms in nearby unit cells to relax to reduce the overall energy. This relaxation provides a mechanism to spread out the energetic effect of a spatially varying $\mathbf{w}$, leading again to an energy density proportional to $(\nabla\mathbf{w})^2$. Atomic positions in distorted structures might be determined as follows: (i) Find the tilings associated with nonuniform $\mathbf{w}$ as shown in Fig. 3(c), (ii) locate atomic positions using the ideal atomic configurations within each cell, and (iii) allow the atoms to relax to the lowest energy configuration without changing the topology of atomic arrangements (i.e., without interchanging positions). This relaxation is presumably a fast, nonhydrodynamic process. One is then left with a distorted configuration with energy density proportional to $(\nabla\mathbf{w})^2$. This configuration can now relax to the state of uniform $\mathbf{w}$ only by rearranging atoms—a slow, diffusive process. This picture is consistent with the elastic and hydrodynamic theories.

In summary, both the discrete and hydrodynamic versions of phason dynamics support the view that $\mathbf{w}$ relaxation is implemented via mass diffusion with a mobility that is of the same order as that for mass diffusion in solids. Since mass diffusion mobilities are extremely small ($<10^{-10}$ cm^2/sec), spatial variations in $\mathbf{w}$ that might be present at the time of preparation relax very slowly and are effectively quenched. This may account for the fact that electron micrographs of icosahedral phases appear to have many jags associated with unrelaxed phason variations.

III. THE CONNECTION BETWEEN DENSITY WAVES AND TILINGS

The purpose of this section is to provide the detailed connection between the hydrodynamic variables ($\mathbf{u}$ and $\mathbf{w}$) of the density-wave picture and the parameters used in the unit-cell constructions. The connection can be determined by examining the relationship between the parameters of the unit-cell construction and the $\rho_{\mathbf{G}}$ (amplitudes and phases) of the peaks in their Fourier transform. The same analysis that derives $\mathbf{u}$ and $\mathbf{w}$ from the phases of $\rho_{\mathbf{G}}$ in the density-wave picture can then be used to derive $\mathbf{u}_t$ and $\mathbf{w}_t$ from the $\rho_{\mathbf{G}}$ and, ultimately, the parameters in the unit-cell picture. Once this connection is made, there is a clear prescription for varying the parameters to obtain tilings with spatially varying phonon and phason variables.

There are several different construction techniques which can be used to generate pentagonal quasicrystal tilings. These include direct projection of a subset of points in a 5D hypercubic lattice,[4,5,13,14] taking the dual of five sets of periodically or quasiperiodically space parallel lines,[3,13] and, in the case of the Penrose tilings, decorating an *Ammann quasilattice*.[12] In this paper, we will use the last technique for most of our discussion for several reasons. First, the Fourier transform of the Ammann quasilattice itself can also be easily calculated and compared to the simple Landau theory. Second, defects in the Ammann quasilattice are readily recognized and analyzed, and since the tiling is just a decoration of the quasilattice, defects in the quasilattice are essentially equivalent to defects in the tiling. Note that a discussion of the quasilattice approach automatically incorporates the dual approach since the tiling can be obtained from the Ammann quasilattice by a generalized dual transform as well as by decoration. Finally, the structure of the Ammann quasilattice explicitly illustrates the two incommensurate periods associated with each orientational direction.

Although our discussion will be centered around the Ammann quasilattice, in some cases the direct projection technique is especially useful (e.g., for producing pictures of tilings) and we will therefore discuss it as well. Both methods can be generalized to 3D icosahedral structures as well as to other symmetries.

A. Ammann quasilattices and their Fourier transforms

An Ammann quasilattice, which can be regarded as a decoration of a Penrose tiling, is a special case of a Fibonacci pentagrid.[12] A Fibonacci pentagrid is composed of five sets of parallel lines, or five "grids;" the unit normals to these lines form a star of vectors with pentagonal symmetry. Each space between successive parallel lines is either a short interval S or a long interval $L=\tau S$, where $\tau=(1+\sqrt{5})/2$. The ordering of L's and S's in each direction forms a Fibonacci sequence. For $S=1$, the equations of the lines in a Fibonacci pentagrid are

$$\mathbf{x}\cdot\mathbf{e}_n = N+\alpha_n+\frac{1}{\tau}\left\lfloor\frac{N}{\tau}+\beta_n\right\rfloor,\quad n=0,\ldots,4\,, \tag{4}$$

where n labels the orientation of the grid line, $\mathbf{e}_n=[\cos(2\pi n/5),\sin(2\pi n/5)]$, N is an integer which indexes the lines in a given direction, and $[z]$ denotes the greatest integer less than or equal to z. The ten real parameters α_n and β_n completely determine the Fibonacci pentagrid.

By the Fourier transform of a Fibonacci pentagrid we mean the Fourier transform of $\sum'\delta(\mathbf{x}-\mathbf{r})$, where $\mathbf{r}$ is a

vector that points to the intersection of a pair of lines and the $\sum'$ is a normalized sum over all $\mathbf{r}$, as discussed in Ref. 23. Setting $T=1+1/\tau^2$, it is useful to define the following quantities:

$$k_{pq}=\frac{2\pi}{T}\left[p+\frac{q}{\tau}\right],$$

$$X_{pq}=\frac{2\pi}{T}\left[q-\frac{p}{\tau}\right],$$

$$\psi_{pq}^{(i)}=\frac{2\pi}{T}\left[\alpha_i\left[p+\frac{q}{\tau}\right]+(\beta_i-\tfrac{1}{2})\left[\frac{p}{\tau}-q\right]\right] \tag{5}$$

$$=\frac{2\pi}{T}[\alpha_i k_{pq}-(\beta_i-\tfrac{1}{2})X_{pq}],$$

and the function

$$f^{(j)}(k)=\begin{cases}\dfrac{\sin(X_{pq}/2)}{X_{pq}/2}\exp(i\psi_{pq}^{(j)}) & \text{for } k=k_{pq}\\ 0, \text{ otherwise}, & \end{cases} \tag{6}$$

where p and q are integers. Then, the Fourier transform of a Fibonacci pentagrid can be written as

$$\rho(\mathbf{k})=\sum_{l<m} f^{(l)}(\mathbf{k}\cdot\mathbf{u}_{lm})f^{(m)}(\mathbf{k}\cdot\mathbf{u}_{ml}), \tag{7}$$

where

$$\mathbf{u}_{lm}\equiv\frac{\mathbf{e}_l-(\mathbf{e}_l\cdot\mathbf{e}_m)\mathbf{e}_m}{1-(\mathbf{e}_l\cdot\mathbf{e}_m)^2}.$$

$\rho(\mathbf{k})$ is nonzero if and only if $\mathbf{k}\cdot\mathbf{u}_{lm}$ is a number of the form of k_{pq} [Eq. (6)]; this constrains $\mathbf{k}$ to equal one of a discrete set of reciprocal vectors, $\mathbf{G}=\sum n_i\mathbf{e}_i$, where $n_i=$integer. Note that $\phi_{\mathbf{G}_n}$ represents the phase of the entire sum in Eq. (7).

If we now interpret $\rho(\mathbf{k})$ as a Fourier sum of density waves, our first task is to determine which values of α_n and β_n yield configurations that are degenerate with respect to the Landau free energy. Recall that the coefficients of the various powers of the density in the free energy expansion depend upon the sums of $\phi_{\mathbf{G}}$ where $\sum\mathbf{G}=0$ [see Eq. (2)].

A shown in Refs. 12 and 23, there are two kinds of transformations of α_n and β_n that leave $|\rho(\mathbf{k})|$ invariant. The first is a discrete transformation known as an "umklapp:"

$$\alpha_n\rightarrow\alpha_n+p_n+q_n/\tau,\quad \beta_n\rightarrow\beta_n-q_n+p_n/\tau, \tag{8}$$

where p_n and q_n are integers; an umklapp leaves $|\rho(\mathbf{k}=\mathbf{G})|\equiv|\rho_{\mathbf{G}}|$ and $\phi_{\mathbf{G}}$ (modulo 2π) unchanged. Therefore, F is unchanged.

The second is a continuous transformation of the form

$$\alpha_n\rightarrow\alpha_n+\mathbf{u}_t\cdot\mathbf{e}_n,\quad \beta_n\rightarrow\beta_n+\mathbf{w}_t\cdot\mathbf{e}_{\langle 3n\rangle}, \tag{9}$$

for arbitrary $\mathbf{u}_t$ and $\mathbf{w}_t$. Such transformations were shown to leave $|\rho_{\mathbf{G}}|$ unchanged; also, if we write $\mathbf{G}=\sum n_i\mathbf{G}_n$ (where $\mathbf{G}_n$ point to the vertices of a pentagon and $n_i=$integer) then

$$\phi_{\mathbf{G}}\rightarrow\phi'_{\mathbf{G}}\equiv\phi_{\mathbf{G}}+\mathbf{G}\cdot\mathbf{u}_t-\overline{\mathbf{G}}\cdot\mathbf{w}_t, \tag{10}$$

where $\overline{\mathbf{G}}\equiv\sum n_i\mathbf{G}_{\langle 3n\rangle}$. Note that, for any set $\{\mathbf{G}\}$ such that $\sum\mathbf{G}=0$, $\sum\phi_{\mathbf{G}}=\sum\phi'_{\mathbf{G}}$. Thus, from Eq. (2), we see that F is not changed under these transformations either.

In summary, all Fibonacci pentagrids of the form

$$\alpha_n=a_n+\mathbf{u}_t\cdot\mathbf{e}_n+p_n+q_n/\tau$$

and (11)

$$\beta_n=b_n+\mathbf{w}_t\cdot\mathbf{e}_{\langle 3n\rangle}-q_n+p_n/\tau$$

(for some specified set $\{a_n,b_n\}$ and arbitrary choices of $\mathbf{u}_t$ and $\mathbf{w}_t$) are completely degenerate from the point of view of the Landau free energy. To specify a preferred ground state for the system one must specify values of a_n and b_n. The choices $a_n=(6\tau-1)/[2(\tau+2)]$ and $b_n=-2/(\tau+2)$ for all n were shown to correspond to the Ammann quasilattices, which, for the purposes of this discussion, we take to be the ground state. This choice corresponds to the choice $\sum\phi_{\mathbf{G}_n}=0$ in the minimal density-wave picture, as can be verified by computing the phase factor according to Eq. (7).

The form of the transformations of Eq. (11) strongly suggests that we identify spatial variations of $\mathbf{u}_t$ in the Ammann quasilattice as phonons ($\mathbf{u}$) and spatial variations of $\mathbf{w}_t$ with phasons ($\mathbf{w}$). We will therefore *drop the subscript* in the remaining discussion. This identification is justified by Eq. (10), where it is explicitly verified that $\mathbf{u}$ affects the phases exactly as a translation would and $\mathbf{w}$ exactly as changes in $\mathbf{w}$ do in the simple Landau theory. In Figs. 4(a)–4(c) we show a perfect Ammann quasilattice (a), an Ammann quasilattice containing variations in $\mathbf{u}$ (b), and one containing variations in $\mathbf{w}$ (c). In these pictures it is quite easy to separate effects due to $\mathbf{u}$ (curvature of the lines) from those due to $\mathbf{w}$ (jags in the lines). The reader is encouraged to copy Fig. 4 on a transparency and overlay it on Fig. 3. Note that each jag in Fig. 4 corresponds to a mismatch in the tiling of Fig. 3.

Phason variation in 3D icosahedral quasicrystals produces line defects. The icosahedral Ammann quasilattice[12] consists of six sets of parallel planes, each plane being perpendicular to a vector pointing to the vertex of an icosahedron. As in the 2D Penrose case, the spacings between elements of a given set form a Fibonacci sequence. The jags induced by linear variations in β are, therefore, discontinuous steps between half-planes (rather than jags between half lines). Mismatches in the unit-cell configuration occur along the edges of these half-planes. More general variations in β will lead to displacements of sections of Ammann planes whose boundaries form closed loops of steps.

B. Generating unit-cell pictures using projections

We have already stated that the pictures of Penrose tilings and pictures of Ammann quasilattices are equivalent in that a tiling is simply a decoration of a quasilattice, and vice versa. By comparing Figs. 4 and 3, we can see how this correspondence can lead to a procedure for producing the pictures of Fig. 3. There is, however, another technique which can be used without reference to the Am-

mann quasilattice and which is easier to implement than the decoration.

It is well known by now that the Penrose tilings can be obtained by orthogonally projecting a subset of the lattice points of a 5D hypercubic lattice onto a particular 2D subspace.[4,13,19] A simple procedure for doing this is as follows: Let $\mathbf{R}$ denote a lattice point in the 5D hypercubic lattice; $\mathbf{R}=\sum n_i \mathbf{f}_i$, where $\mathbf{f}_i$ are the basis vectors of the hypercubic lattice. Project $\mathbf{R}$ onto the 3D subspace orthogonal to the tiling plane using the matrix $\mathbf{P}^{\perp}_{ij}=\frac{1}{5}\cos[4\pi(j-i)/5]+\frac{1}{5}$. If the projected point $\mathbf{P}^{\perp}\mathbf{R}$ lies within the image of the unit cube (with its lowest index corner at the origin) under the same projection, then project $\mathbf{R}$ onto the tiling plane using the matrix $\mathbf{P}^{\parallel}_{ij}=\frac{1}{5}\cos[2\pi(j-i)/5]$. Do this for every $\mathbf{R}$ and then join, by a line segment in the tiling plane, any pair of points whose positions differ by a single $\mathbf{e}_i$, where $\mathbf{e}_i=\mathbf{P}^{\parallel}_{ij}\mathbf{f}_j$. (The five $\mathbf{e}_i$'s form a star of vectors with pentagonal symmetry.)

Different tilings can be formed in this manner by adding a constant vector $\boldsymbol{\gamma}$ (with components γ_n, where $n=0,\ldots,4$) to each $\mathbf{R}$ before carrying out the projection procedure. Shifts in $\boldsymbol{\gamma}$ correspond to five degrees of freedom in generating the tiling. One degree of freedom, the component of $\boldsymbol{\gamma}$ in the (1,1,1,1,1) direction is associated with shifts in LI class. More specifically, an LI class is determined by the value of $\gamma^{\mathrm{LI}}\equiv \mathrm{mod}_1\boldsymbol{\gamma}\cdot(1,1,1,1,1)$. The Penrose LI class corresponds to $\gamma^{\mathrm{LI}}=0$.

Varying γ^{LI} spans a continuous (uncountable) set of LI classes; however, even this is only a highly restricted subset of all possible LI classes. For example, by projecting from yet higher dimensional lattices, where there are even more degrees of freedom, other LI classes can be generated. The existence of more LI classes was already pointed out in the discussion of the generalized dual method in Ref. 3, where it is demonstrated that they can be easily generated by using different kinds of quasiperiodic grids.

A variation in the phonon field, as we have seen, is given by $\Delta\alpha_n=\mathbf{u}\cdot\mathbf{e}_n$, and a variation in the phason field by $\Delta\beta_n=\mathbf{w}\cdot\mathbf{e}_{\langle 3n\rangle}$. These imply $\Delta\gamma_n^{\mathrm{phonon}}\propto\mathbf{u}\cdot\mathbf{e}_n$ and $\Delta\gamma_n^{\mathrm{phason}}\propto\mathbf{w}\cdot\mathbf{e}_{\langle 3n\rangle}$. It is easily verified that

$$\begin{aligned}&\mathbf{P}^{\parallel}\Delta\boldsymbol{\gamma}^{\mathrm{phonon}}=\Delta\boldsymbol{\gamma}^{\mathrm{phonon}},\quad \mathbf{P}^{\perp}\Delta\boldsymbol{\gamma}^{\mathrm{phonon}}=0\,,\\ &\mathbf{P}^{\parallel}\Delta\boldsymbol{\gamma}^{\mathrm{phason}}=0,\quad \mathbf{P}^{\perp}\Delta\boldsymbol{\gamma}^{\mathrm{phason}}=\Delta\boldsymbol{\gamma}^{\mathrm{phason}}\,,\end{aligned}\tag{12}$$

i.e., phonon variations correspond to changes of $\boldsymbol{\gamma}$ in the tiling plane and phasons to changes in the orthogonal subspace.

The projection and Ammann quasilattice approaches are related in the following sense: The Penrose tiling associated with a given Ammann quasilattice is given by the projection method with

$$\gamma_n=\left[1+\frac{1}{\tau^2}\right]^{-1}[\alpha_n+(\beta_n-\tfrac{1}{2})/\tau]\,,\tag{13}$$

where γ_n is the nth component of $\boldsymbol{\gamma}$.[12] Given values of α_n and β_n corresponding to an Ammann quasilattice, one can generate the Penrose tiling associated with them using Eq. (13) and the projection technique. To obtain a tiling where α_n and β_n are spatially varying, a spatially varying $\boldsymbol{\gamma}$ must be added to each $\mathbf{R}$ associated with the higher-dimensional lattice points according to the position in the tiling plane of $\mathbf{P}^{\parallel}\mathbf{R}$.

C. Ammann quasilattices, phasons, and worms

We next will examine the effect of a spatially varying phason variable or, equivalently, a spatially varying β_n on the Ammann quasilattice and the Penrose tiling associated with it. A complete discussion of this topic must include two distinct issues: (i) the effect of a change in β_n on the nth grid, and (ii) the way in which changes in the individual grids are coupled by the conditions of Eq. (11) and the consequent effect on the tilings. The first issue is treated at length in Sec. V; we will first discuss the second issue, anticipating a few simple results from Sec. V (which are obvious from Fig. 4).

As detailed in Sec. V and displayed in Fig. 4, the effect of a small uniform shift in β ($\Delta\beta<1$) on a given grid is to shift the position of some of the lines in the grid. According to Eq. (4), if the value of $\lfloor N/\tau+\beta\rfloor$ is changed by the shift in β, then the Nth line in the grid is shifted by $\pm 1/\tau$. To see the effect of this shift on the tiling we make use of the fact that a Penrose tiling can be obtained from its Ammann quasilattice by a generalized dual transformation, as well as by decoration.[12] To see that shifting a line can cause a worm to flip, one need only examine the way in which the Ammann lines decorate a worm (see Fig. 5). If an Ammann line parallel to a worm is shifted by precisely $1/\tau$ to the other side of the worm, it causes a rearrangement of all the Ammann line intersections just such that the dual construction applied to the new intersections produces the same worm outline with all the internal hexagons flipped. Furthermore, flipping a worm segment is the only tiling rearrangement which corresponds to a shift by $1/\tau$ in an Ammann quasilattice line. Thus, all shifts induced by changes in $\mathbf{w}_t$ *must* occur along worms. Where two or more worms cross, the worms must flip in a specific order, determined by the order in which the relevant values of $N/\tau+\beta_n$ cross an integer as $\mathbf{w}_t$ is smoothly varied.

Using the fact that the dual to an undefected Ammann quasilattice is a Penrose tiling, we are able to study the effect of spatial variations in the phason field $\mathbf{w}$ in terms of Penrose matching rule violations. First, since no local defects in the Ammann quasilattice are induced by these variations except at the points where jags occur, there can be no mismatches in the tiles except at these isolated points. Second, since these points always occur within worms (or where worms cross) the mismatches must occur at the common edge shared by two hexagons along a worm. Finally, it is clear that mismatches along a given direction cannot be removed except by annihilation with another mismatch in the same direction, i.e., by having the two jags at the ends of a shifted segment of an Ammann line brought together so that the segment shrinks to zero length. Bringing the two jags together corresponds to successively flipping hexagons between the two ends of the worm in the dual tiling. (In 3D, the mismatches form either open curves that annihilate or a closed loop which can shrink to zero length.) Thus, a spatially varying phason field relaxes through a series of local rearrange-

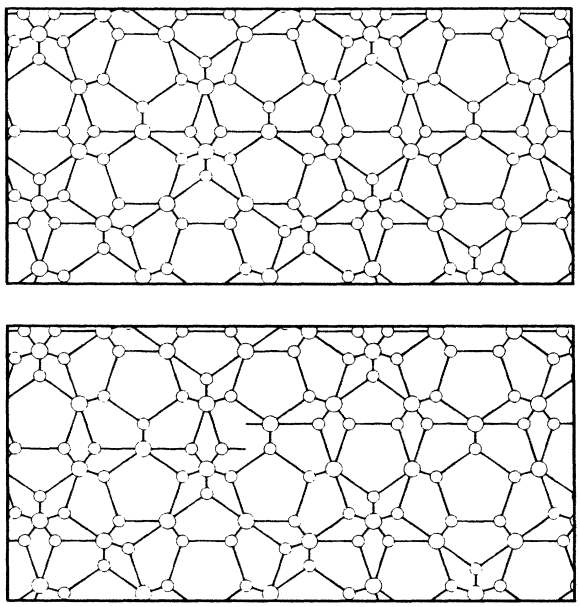

FIG. 8. Illustration of a phason-induced mismatch in a toy atomic model. The two unit cells of a Penrose tiling have been decorated with atoms and bonds to produce a covalently bonded structure containing four types of atoms. Each is always found in the same bonding configuration. (a) The preferred arrangement of atoms (a perfect tiling). (b) The effect on the atomic structure of a phason-induced mismatch. Near the center of the picture is a dangling bond indicating a deviation from the perfect structure. Note that while an entire slice of atoms has been flipped over [compare to (a)], all bonds are intact except the one at the center. This configuration can relax to that of (a) through a series of local switches in atomic positions.

ments of unit cells, or, equivalently, atoms or atomic clusters in a real material. (See Fig. 8 for an image of what such rearrangements mean in terms of an atomic decoration.)

IV. DISLOCATIONS

To describe a dislocation in a Penrose tiling, we will consider $\mathbf{u}$, $\mathbf{w}$, α_n, and β_n to be functions of the polar angle θ (measured about the dislocation core). The functions $\alpha_n(\theta)$ and $\beta_n(\theta)$ associated with a dislocation must satisfy the following restrictions.

(i) There must exist $\mathbf{u}(\theta)$ and $\mathbf{w}(\theta)$ such that $\alpha_n(\theta)=\mathbf{u}(\theta)\cdot\mathbf{e}_n+\text{const}$ and $\beta_n(\theta)=\mathbf{w}(\theta)\cdot\mathbf{e}_{\langle 3n\rangle}+\text{const}$ [see Eq. (11)]. This guarantees that as $r\rightarrow\infty$ the pattern approaches a perfect Ammann quasilattice (i.e., a pattern in the same LI class as the undefected lattice) for all values of θ other than 0.

(ii) The values of $\alpha_n(2\pi)$ and $\beta_n(2\pi)$ must be related to $\alpha_n(0)$ and $\beta_n(0)$ by an umklapp for all n. This guarantees that there will be no defects along the $\theta=0$ ray.

The Burgers vector lattice is determined by the values of $\Delta\mathbf{u}\equiv\mathbf{u}(2\pi)-\mathbf{u}(0)$ and $\Delta\mathbf{w}\equiv\mathbf{w}(2\pi)-\mathbf{w}(0)$ that are consistent with restriction (ii). These imply that

$$\Delta\mathbf{u}\cdot\mathbf{e}_n=P_n+Q_n/\tau$$

and (14)

$$\Delta\mathbf{w}\cdot\mathbf{e}_{\langle 3n\rangle}=-Q_n+P_n/\tau$$

for some set of integers P_n and Q_n. Solutions can be found for these ten equations only if certain relations hold among the P_n's and Q_n's. The simplest solutions that satisfy these equations are of the form

$$\begin{aligned}&P_i=0,\ P_{i+1}=1,\ P_{i+2}=0,\ P_{i+3}=0,\ P_{i+4}=-1\ ,\\ &Q_i=0,\ Q_{i+1}=0,\ Q_{i+2}=1,\ Q_{i+3}=-1,\ Q_{i+4}=0\end{aligned} \tag{15}$$

for any i, where all indices are taken modulo 5. These correspond to

$$\mathbf{u}=\frac{1}{\sin(2\pi/5)}\mathbf{e}_i^r$$

and (16)

$$\mathbf{w}=\frac{-1}{\sin(4\pi/5)}\mathbf{e}^r_{\langle 3i\rangle}\ ,$$

where $\mathbf{e}_i^r$ is a unit vector corresponding to a counterclockwise rotation of $\mathbf{e}_i$ through 90°. We term these "fundamental dislocations." Any dislocation can be composed as an integer linear combination of these fundamentals. Note that only four of the fundamental dislocations are independent, so that the Burgers vector lattice is four dimensional, in agreement with the density-wave analysis. In fact, Eq. (16) picks out exactly the same Burgers vector lattice as was derived from the density-wave analysis.[9]

The effect on the $\phi_{\mathbf{G}_n}$ and $\phi_{\mathbf{G}'_n}$, the phases of the diffraction peaks with wave vectors $\mathbf{G}_n$ and $\mathbf{G}'_n\equiv(1/\tau)\mathbf{G}_n$ (see Sec. II B 4), induced by a fundamental dislocation is particularly simple. Let $\Delta\phi=\phi(2\pi)-\phi(0)$. From Eq. (10) we have $\Delta\phi_{\mathbf{G}}=\mathbf{G}\cdot\mathbf{u}+\bar{\mathbf{G}}\cdot\mathbf{w}$. A straightforward calculation reveals that

$$\Delta\phi_{\mathbf{G}_n}=2\pi P_n \text{ and } \Delta\phi_{\mathbf{G}'_n}=2\pi Q_n\ . \tag{17}$$

A variation in the phase of a single spot in the Landau theory corresponds to a partial dislocation (as in the case of a periodic crystal). Only one of the $\phi_{\mathbf{G}_n}$ or $\phi_{\mathbf{G}'_n}$ is affected if $P_i=1$ for some i with all other P_j and Q_j equal to zero—corresponding to a P-type partial (or $Q_i=1$ for some i with all other P_j and Q_j equal to zero—corresponding to a Q-type partial). A fundamental dislocation can be seen to consist of two P-type and two Q-type partials. We discuss the nature of these partials in detail in Sec. V. Every dislocation must contain at least two partials in $\{\mathbf{G}_n\}$ and two in $\{\mathbf{G}'_n\}$. (It is easy to see that any integer linear combination of the fundamentals for which $Q_n=0$, $\forall n$ also has $P_n=0$, $\forall n$ and is therefore not a defect at all. At least two of the Q's and two of the P's must be nonzero in order to satisfy the constraint on the sums of the phases in each ring.)

The Burgers vectors and the structure of a dislocation have simple interpretations in the 5D hypercubic lattice from which the Penrose tilings can be projected. To see this we simply compute the vector $\gamma(2\pi)$ associated with $\alpha_n(2\pi)$ and $\beta_n(2\pi)$ according to Eq. (13). The result is

that $\gamma_n(2\pi)$ is an integer for all n and all Burgers vectors and that $\gamma(2\pi)\cdot(1,1,1,1,1)=0$ as expected from Sec. III B. In the hypercubic lattice there is a 3D core perpendicular to the tiling plane about which the angle θ is defined. A dislocation in the projected tiling is obtained by making a standard dislocation in the hypercubic lattice with a Burgers vector perpendicular to the (1,1,1,1,1) direction. This is how Fig. 3(d) was produced. More specifically, in Fig. 3(d) the 5D lattice points considered as candidates for projection were $\mathbf{R}+(\theta/2\pi)(0,1,0,0,-1)$.

V. TOPOLOGICAL DEFECTS IN SINGLE GRIDS

The partial dislocations described in Sec. IV correspond to a change in a single grid, leaving the other four grids in the pentagrid unaltered. Such a defect is not a full dislocation because restriction (i) (in Sec. IV) is not satisfied. We have seen that there exist two distinct types of partials, one corresponding to a change which gives $P=1$, $Q=0$, the other having $P=0$, $Q=1$.

Since all of our results in this section apply to a wider class of grids than the Fibonacci grids that compose the Ammann quasilattice, we have chosen to develop the analysis for the general case. We study grids of parallel lines perpendicular to the x axis whose intersections with that axis are given by

$$x_N=N+\alpha+\rho\lfloor N\sigma+\beta\rfloor\ , \tag{18}$$

where N runs over the integers, σ is an irrational number between 0 and 1, ρ is a nonzero real number, α and β are arbitrary real numbers, and $\lfloor\ \rfloor$ denotes the greatest integer function. Note that the quantity x_N-x_{N-1}, the interval between successive lines, must take on one of two values—either equal to 1 or $1+\rho$. The quasiperiodic grid can thus be thought of as a 1D tiling consisting of two types of tiles with lengths in the ratio $1:1+\rho$.

The Fourier transform $f(k)$ of the grid defined by Eq. (18) consists of a dense set of Bragg peaks along the x direction which can be indexed by two integers, p and q, and can be derived analytically:[23]

$$f(k_{pq})=\exp(i\phi_{pq})\frac{\sin(X_{pq}/2)}{X_{pq}/2}\ ,$$

where

$$\begin{aligned} T&\equiv 1+\rho\sigma\ ,\\ k_{pq}&=\frac{2\pi}{T}(p+q\sigma)\ ,\\ X_{pq}&=\frac{2\pi}{T}(q-p\rho)\ ,\\ \phi_{pq}&=\frac{2\pi}{T}[\alpha(p+q\sigma)+(\beta-\tfrac{1}{2})(p\rho-q)]\ . \end{aligned} \tag{19}$$

Note that the positions of all the peaks can be obtained as integer linear combinations of two fundamental wave vectors, the natural choice for these being $k_{10}=2\pi/T$ and $k_{01}=(2\pi/T)\sigma$.

The simplest Landau description of this grid consists of density waves with these two fundamental wave vectors only with amplitudes given by Eq. (19). This is, of course, precisely equivalent to the Landau theory for a conventional 1D incommensurate smectic which has been studied in some detail.[25] The two degrees of freedom in the system (derived from the independent phases of the individual waves) can be characterized as a phonon field u, and a phason field w. A uniform change in u corresponds to a translation of the entire density, i.e., the maxima of both density waves are translated by the same amount. A uniform change in w corresponds to a relative shift between the positions of the two waves that leaves u fixed.

From Eq. (18), it is clear that α plays the role of the translation variable u, since shifting α shifts all the x_N by the same distance. A uniform change $\Delta\alpha$ shifts the phase ϕ_{pq} by $\Delta\phi_{pq}=(2\pi/T)(p+q\sigma)\Delta\alpha=k_{pq}\Delta\alpha$, just as one expects for a translation. A pure phason (w) variation corresponds to a shift in β with α held fixed. A shift in β shifts the k_{10} wave by $-\rho\Delta\beta$ and the k_{01} by $+\Delta\beta/\sigma$.

In Fig. 9 we illustrate the effects of uniform changes of α and β on a grid. Any horizontal line in either part of the figure intercepts a set of points x_N that forms a perfect sequence defined by Eq. (18) with fixed α and β. In Fig. 9(a), α is made a linear function of y and β is held constant. In Fig. 9(b), α is constant and β varies linearly with y. The breaks in the lines of constant N, henceforth called "jags," due to variations in β occur where the value of $N\sigma+\beta$ crosses an integer. It is clear from these pictures that a change in α simply translates the sequence of intervals while a change in β causes certain rearrangements of it. It is easy to compute various properties of the distribution of jags produced by a given $\Delta\beta$. For example, if β changes monotonically by 1 between two

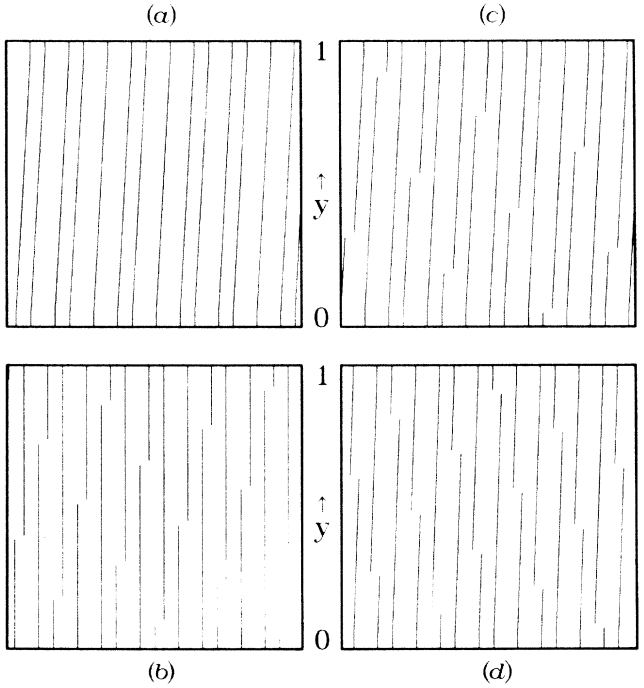

FIG. 9. (a) Effect of linear variation of α on a single grid ($\alpha=cy$). (b) Effect of linear variation of β on a single grid ($\beta=cy$). (c) Effect of linear variation of γ_p on a single grid ($\gamma_p=y$). Note that the sequence at $y=1$ is identical to that at $y=0$. (d) Effect of linear variation of γ_q on a single grid ($\gamma_q=y$). As in (c), the $y=1$ and $y=0$ sequences are identical.

values of y there must be one jag between those y values for each value of N.

While α and β are the variables most closely related to the u and w of the Landau theory, it turns out to be more useful to discuss defects using the variables $\gamma_p \equiv [\alpha+(\beta-\frac{1}{2})\rho]/T$ and $\gamma_q \equiv [\alpha\sigma-(\beta-\frac{1}{2})]/T$. Note that ϕ_{pq} can be written in terms of these as

$$\phi_{pq}=2\pi(\gamma_p p+\gamma_q q)\ . \tag{20}$$

The significance of γ_p and γ_q in the density-wave picture is obvious: changes in γ_p (γ_q) correspond to motion of the k_{10} (k_{01}) wave with the other held fixed. The importance of these variables in the tiling case stems from the following property of the sequence x_N: There is a transformation of α and β, called an *umklapp*,[12] which takes x_N to x'_N where $x'_N=x_{N+p}$. The set of positions x_N remains unaltered under an umklapp, but the elements are reindexed. The general umklapp transformation is

$$\Delta\alpha=P+Q\rho,\quad \Delta\beta=P\sigma-Q,\quad P,Q\in\mathbf{Z}\ . \tag{21}$$

The behavior of γ_p and γ_q under umklapps is particularly simple:

$$\begin{aligned}\Delta\gamma_p&=\frac{1}{T}(\Delta\alpha+\Delta\beta\rho)=P\ ,\\ \Delta\gamma_q&=\frac{1}{T}(\Delta\alpha\sigma-\Delta\beta)=Q\ .\end{aligned} \tag{22}$$

It follows immediately from this and Eq. (20) that ϕ_{pq} changes by an integral multiple of 2π under umklapps. As expected, the Fourier transform is unaffected.

In Figs. 9(c) and 9(d) we illustrate the effects of linear variations in γ_p and γ_q on a grid. Note that as γ_q changes by 1 each line of constant N must contain exactly 1 jag. ($\Delta\gamma_q=1$, $\Delta\gamma_p=0\Rightarrow\Delta\beta=-1$, which means that $[N\sigma+\beta]$ must change by 1 regardless of the value of N.) A net change by 1 in γ_p, on the other hand, produces σ (<1) jags per line on the average. We emphasize that in either case the final ($y=1$) sequence is identical to the initial ($y=0$) sequence.

A grid containing defects can be described as the set of points that satisfies the equation $x=N+\alpha(x,y)+\rho[N\sigma+\beta(x,y)]$ for some integer N, the basic, undefected grid being one for which $\alpha(x,y)$ and $\beta(x,y)$ are constant. Having already seen, in Fig. 9, the effect on a grid of linear variations of α and β, we now consider variations in α and β that are topologically inequivalent to the undefected grid. When referring to a single grid only (and not an entire pentagrid, say), we will refer to such variations as dislocations. Recall that such a variation in a single grid corresponds to a partial dislocation when referring to an entire pentagrid.

A dislocation at the origin can be constructed by making α and β smooth functions of the polar angle θ and requiring that the sequence formed at $\theta=0$ be equivalent to the sequence at $\theta=2\pi$; i.e., these two sequences must be identical up to umklapps. There are two simple ways to meet this condition, one by choosing $\alpha(\theta)$ and $\beta(\theta)$ such that $\gamma_p(2\pi)-\gamma_p(0)=P$ and $\gamma_q(\theta)=\text{const}$, the other such that $\gamma_q(2\pi)-\gamma_q(0)=Q$ and $\gamma_p(\theta)=\text{const}$. Figure 10 illustrates these two types of defects for the cases (a) $P=1$ and (b) $Q=1$. We call these P-type and Q-type dislocations, respectively. From Eq. (20) we see that in the P-type dislocation, the phase ϕ_{10} of the k_{10} peak changes by 2π as a path enclosing the origin is traversed, while the phase ϕ_{01} is unaffected. Similarly, in the Q-type dislocation, ϕ_{01} changes by 2π while ϕ_{10} is constant.

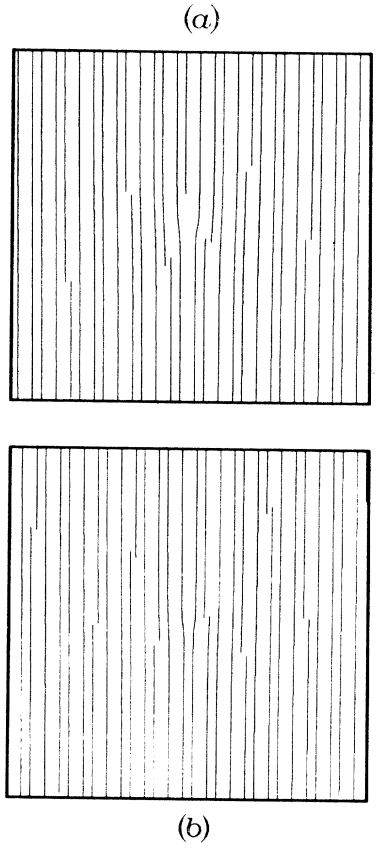

FIG. 10. (a) A P-type dislocation in a single grid. Note the presence of an extra half line in the top half of the picture, terminating at the core. (b) A Q-type dislocation in a single grid. In this case there is no extra half line. Nonetheless, this defect is topologically stable.

There is a significant difference between the P-type and Q-type dislocations as they appear in the discrete grid picture. This difference is due to the fact that the k_{01} has a different kind of source from that of the k_{10} peak. The positions of the grid lines given in Eq. (18) can be reexpressed as

$$\begin{aligned}x_N&=NT+\alpha+\beta\rho-\rho\left\{\frac{\sigma}{T}(NT+\alpha+\beta\rho)-\frac{1}{T}(\alpha\sigma-\beta)\right\}\\ &=T(N+\gamma_p)+\frac{\rho}{2}-\rho\left\{\frac{\sigma}{T}((N+\gamma_p)T)-\gamma_q+\frac{1}{2T}\right\},\end{aligned} \tag{23}$$

where $\{x\}$ is the fractional part of x, and γ_p, γ_q, and T are defined as above. The first term in this expression increases steadily with N, while the last simply varies between 0 and 1.

In this form the quasiperiodic grid is conveniently in-

terpreted as a periodic grid of lines with period T (the first term) modulated by a periodic function with period T/σ (the last term). The k_{10} peak (period T) is associated with the periodic grid itself, while the k_{01} peak (period T/σ) is associated with the modulation of the grid. In the pictures of the two types of dislocations (Fig. 10) this difference has an immediate and visible consequence. The P type involves the removal (or insertion) of half a line in the grid, while the Q type contains only jags with no extra half line. This difference can also be traced to the fact that a P-type umklapp reindexes the lines in a grid while the Q-type one does not.

The distribution of jags in a pattern with a dislocation can depend on the specific form chosen for $\gamma_p(\theta)$ and $\gamma_q(\theta)$. For example, if one of these is a linear function of θ and the other a constant, the dislocations pictured in Fig. 10 result. In general, as a circle of radius r about the origin is traversed, a net change in β occurs whose value is determined solely by the topological character of the defect. ($\Delta\beta=1$ in the Q-type case and $\Delta\beta=\sigma$ in the P-type case.) Since this change is independent of the value of r, the average number of jags at a given radius is also independent of r.[27] The density of jags therefore goes like $1/r$ and the total number of jags like L, where L is the length of the system. In any local region, the density of jags is proportional to the gradient in β or, equivalently, the gradient in the phason field w. If we associate a finite energy with each jag (which, it may be recalled, is associated with a mismatch in the Penrose tiling), then there is a contribution to the energy of a dislocation that is proportional to $\int |\nabla w| \propto L$, where the integral is over the sample. This result from the unit-cell description differs from the standard elasticity result which predicts a phason contribution proportional to $\int (\nabla w)^2 \propto \ln L$. See Sec. II C for a more complete discussion of the physical significance of these results.

VI. CONCLUSIONS

The principal goal of this paper has been to relate the unit-cell and density-wave descriptions to form a unified theory of quasicrystal structure. Some remarks are in order concerning the relation of this work to current experiments. While the nature of defects in quasicrystal tilings is an interesting subject in its own right, the authors were also motivated by the possible relevance of this analysis to the recently discovered icosahedral phase of Al-Mn and related alloys. In this regard, the most important result of the analysis is a clearer understanding of the nature of phasons in quasicrystal structures. Whereas previous treatments of incommensurate systems considered phasons only as relative shifts in the phases of incommensurate density waves, we now have a microscopic (or atomic) model of phasons in quasicrystals.

In terms of density-wave images (or, equivalently, electron micrographs), we have shown that a spatial variation in the phason variable results in jags in the lines connecting the high-density regions, whereas variations in the phonon variable produce curvature without jags in the lines. This result has immediate experimental relevance since many electron micrographs of the icosahedral phase of Al-Mn and related alloys show the jags (without curvature),[17] representing clear evidence of quenched strains in the phason variable. In terms of the unit-cell picture, we have shown that spatial variations or strains in phason variable correspond to special rearrangements (without distortion) of the unit cells and that such strains can relax by local rearrangements of the unit cells. We have discussed two plausible descriptions of the dynamics of phason relaxation, both of which involve local diffusion of atoms. Since diffusion is very slow compared to phonon relaxation, processes such as dislocation motion and annihilation or relaxation of phason strains take place over long time scales.[10] These observations also answer one of the criticisms of the quasicrystal model which suggests that mismatches produced during rapid aggregation of unit cells may inhibit quasicrystal growth. Such mismatches correspond to phason strains which do not represent a significant impediment to quasicrystal growth since their energetic cost is small and they can relax in a smooth way through local rearrangements of atoms.

These results may be useful in explaining several experimentally measured properties of rapidly quenched icosahedral phases that deviate from the predictions of the ideal quasicrystal model. If phason relaxation is a slow process, as we have argued, then it might be expected that phason strains would be quenched when the samples are rapidly solidified. The fact that jags are observed in electron micrographs is direct evidence supporting this hypothesis. (The variation in the phonon variable should relax quickly to its equilibrium value in the presence of the phason strain. The absence of significant curvature in the electron micrographs suggests that the elastic constant coupling phonons and phasons is small.) Strains in the phason variable can also produce intrinsic broadening of the diffraction peaks which does not vary uniformly with wave number.[28] Broadening that varies nonuniformly with wave number has been observed in x-ray powder diffraction.[29] Furthermore, anisotropic strains in the phason variable have been shown to produce nonuniform shifts and anisotropic broadening of the diffraction peaks, as might be observed in electron diffraction experiments.[28] Recently, such nonuniform shifts have been observed in careful measurements of low-intensity diffraction peaks in the icosahedral phase of rapidly quenched alloys.[28,30] Thus, the quasicrystal model for the icosahedral phase, which naturally predicts slow relaxation of phason strains, leads to a simple explanation for a number of different experimental observations.

ACKNOWLEDGMENTS

J.E.S.S. was supported by IBM. T.L.C. was supported in part by the National Science Foundation (NSF) under Grant No. DMR-85-40332. P.J.S. was supported by IBM Research and by the NSF Materials Research Laboratory program under Grant No. DMR-82-16718.

[1]D. S. Shectman, I. Blech, D. Gratias, and J. W. Cahn, Phys. Rev. Lett. **53**, 1951 (1984).
[2]D. Levine and P. J. Steinhardt, Phys. Rev. Lett. **53**, 2477 (1984).
[3]J. E. S. Socolar, P. J. Steinhardt, and D. Levine, Phys. Rev. B **32**, 5547 (1985); F. Gahler and J. Rhyner, J. Math. Phys. A **19**, 267 (1986).
[4]M. Duneau and A. Katz, Phys. Rev. Lett. **54**, 2688 (1985).
[5]P. A. Kalugin, A. Kitaev, and L. Levitov, Pis'ma Zh. Eksp. Teor. Fiz. **41**, 100 (1985) [JETP Lett. **41**, 120 (1985)].
[6]P. Bak Phys. Rev. Lett. **54**, 1517 (1985); Phys. Rev. B **32**, 5764 (1985).
[7]S. Troian and N. D. Mermin, Phys. Rev. Lett. **54**, 1524 (1985).
[8]J. Jaric, Phys. Rev. Lett. **55**, 607 (1985).
[9]D. Levine, T. C. Lubensky, S. Ostlund, S. Ramaswamy, P. J. Steinhardt, and J. Toner, Phys. Rev. Lett. **54**, 1520 (1985).
[10]T. C. Lubensky, S. Ramaswamy, and J. Toner, Phys. Rev. B **32**, 7444 (1985); Phys. Rev. B (to be published).
[11]R. Penrose, Bull. Inst. Math. Appl. **10**, 266 (1974).
[12]J. E. S. Socolar and P. J. Steinhardt (unpublished).
[13]N. de Bruijn, Ned. Akad. Weten. Proc. Ser. A **43**, 39 (1981); **43**, 53 (1981).
[14]V. Elser, Acta Cryst. A **42**, 36 (1986).
[15]R. K. P. Zia and W. J. Dallas, J. Phys. A **18**, L341 (1985).
[16]P. Kramer and R. Neri, Acta Cryst. A **40**, 580 (1984).
[17]See, for example, K. Hiraga, M. Hirabayashi, A. Inoue, and T. Masumoto, Sci. Rep. Res. Inst. Tohoku Univ. A **32**, 309 (1985).
[18]M. Kleman, Y. Gefen, and A. Pavlovitch, Europhys. Lett. **1**, 61 (1986).
[19]D. Frenkel, C. L. Henley, and E. D. Siggia (unpublished); P. Bak (private communication).
[20]The notion of phason relaxation through discrete transformations is similar to the ideas expressed in Ref. 17. Unlike Frenkel *et al.*, however, we do not conclude that phasons do not exist in this limit. Phason relaxation can still be a slow, diffusive process.
[21]V. Elser, Phys. Rev. Lett. **54**, 1730 (1985).
[22]In the case of a standard edge dislocation in an isotropic solid the energetically preferred phase variation goes like $\theta + A\cos 2\theta$.
[23]D. Levine and P. J. Steinhardt (unpublished).
[24]See B. Grunbaum and G. C. Shephard, *Tilings and Patterns* (Freeman, San Francisco, in press) for a discussion of Ammann's results.
[25]For a review, see P. Bak, Rep. Prog. Phys. **45**, 587 (1981); and V. L. Pokrovsky and A. L. Talopov, *Theory of Incommensurate Crystals, Sov. Science Reviews,* (Horwood, Zurich, Switzerland, 1985).
[26]M. Peyrard and S. Aubry, J. Phys. C **16**, 1593 (1983).
[27]This average can be regarded as an ensemble average over all dislocations with the same forms of γ_p and γ_q but different values of $\gamma_p(0)$ and/or $\gamma_q(0)$. Since the energies of each of the elements of the ensemble must have the same L dependence, our conclusion about the L dependence of each individual element is justified. Alternatively, the average can be regarded as suitably coarse-grained average over annular regions.
[28]T. C. Lubensky, J. E. S. Socolar, P. J. Steinhardt, P. A. Bancel, and P. A. Heiney (unpublished).
[29]P. A. Bancel, P. A. Heiney, P. W. Stephens, A. I. Goldman, and P. M. Horn, Phys. Rev. Lett. **54**, 2422 (1985).
[30]P. A. Bancel and P. A. Heiney (unpublished).

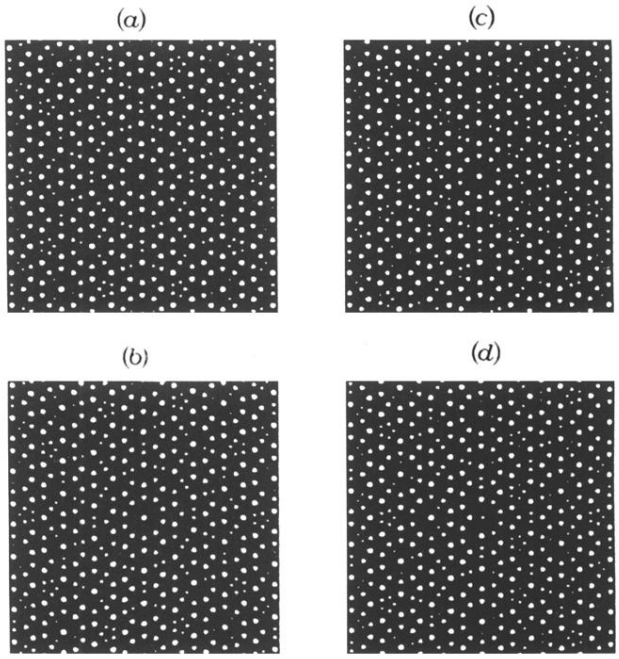

FIG. 1. Density-wave images. A white dot is placed at all points $\mathbf{r}$ where the value of $\rho(\mathbf{r})$ exceeds $\frac{2}{5}$ of its maximum value. (a) A perfect pattern with $\sum \phi_{\mathbf{G}_n} = 0$. (b) A distortion of pattern (a) corresponding to spatial variations in the phonon degree of freedom $\mathbf{u}$. (c) A pattern containing variations in the phason degree of freedom $\mathbf{w}$ about the value used in pattern (a). (d) A dislocation. Note that both phonon variations (curvature) and phason variations (jags) are present.

(a)

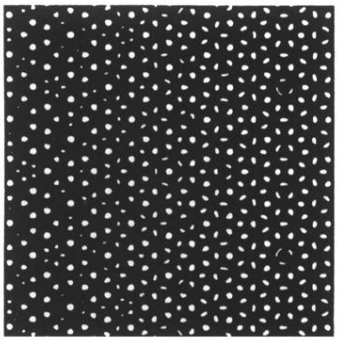

(b)

FIG. 2. Density-wave images. (a) A perfect pattern with $\sum \phi_{G_n} = 0.3$. (b) A pattern in which $\sum \phi_{G_n}$ varies linearly from zero on the left to 0.5 on the right. Variations in $\sum \phi_{G_n}$ correspond to variations in local isomorphism class in the unit-cell picture.

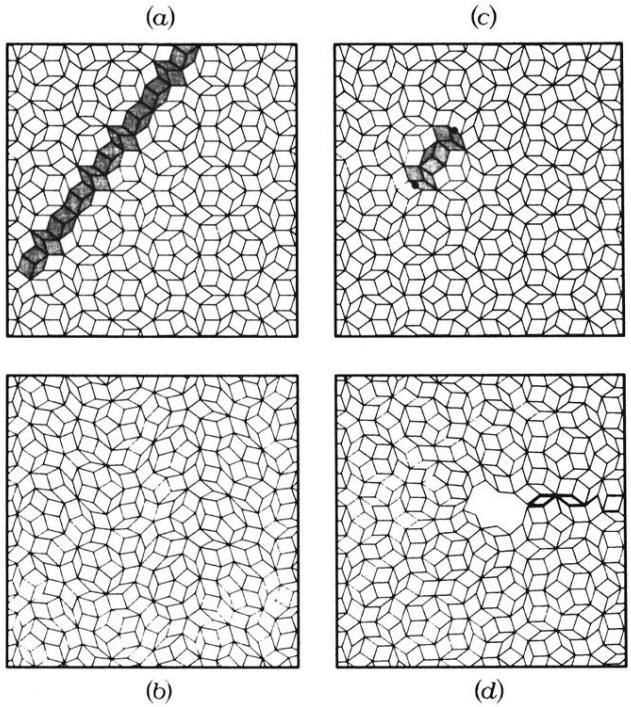

FIG. 3. Penrose tilings. (a) A portion of a perfect Penrose tiling. The shaded unit cells compose a segment of a "worm." (b) A distortion of the tiling of (a) corresponding to variations in the phonon degree of freedom $\mathbf{u}_t$. The unit-cell shapes are distorted, but their arrangement is the same as in (a). (c) A tiling containing variations in the phason degree of freedom $\mathbf{w}_t$ about the value used in (a). The shaded rhombuses form a flipped segment of a worm. [Compare to same region of (a). For more details on worm flips, see Fig. 5.] The large dots at the ends of the shaded segment indicate edges along which the Penrose matching rules are violated—deviations from the Penrose local isomorphism class. This picture contains several other such mismatches and flipped worm segments. To find them, use Fig. 4 as a guide. (d) A dislocation in a Penrose tiling. At large distances from the core the distortion of the unit cells and the density of mismatches both become small, although neither can be completely eliminated.

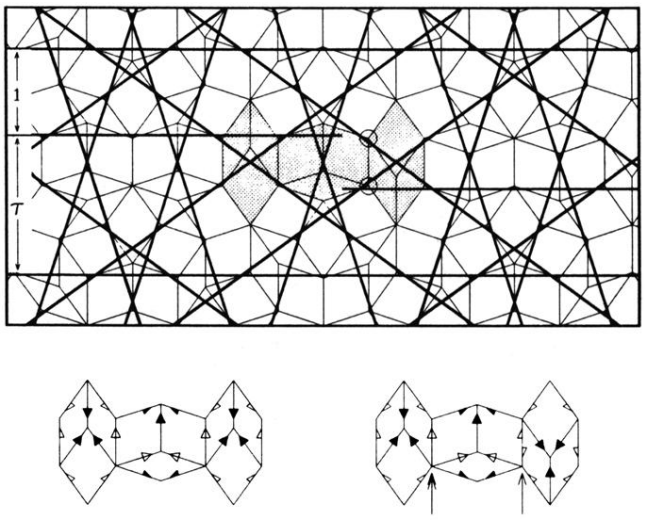

FIG. 5. Illustration of a "worm" in a Penrose tiling and its signature in the Ammann quasilattice. An open circle indicates a type of vertex that is never found in undefected tilings of the Penrose local isomorphism class. The right (left) half of the broken Ammann line can be shifted up (down) to restore the ideal quasilattice in the region depicted. The consequent rearrangements of the intersections of the Ammann quasilattice cause the right (left) half of the worm to flip when the generalized dual technique is applied. The worm segments depicted below are decorated to illustrate the Penrose matching rules. The rules are that two tiles can join only along edges which have the same color arrow pointing in the same direction. The segment on the right corresponds to the shaded segment above, where the rightmost hexagon (formed from one thick and two thin rhombuses) has been flipped, causing a matching rule violation (indicated by the single arrow). If the middle hexagon were now flipped to relieve that mismatch, a mismatch would arise along the edge indicated by the double arrow. Note, however, that the top and bottom of the hexagon are decorated in the same way, so that no other mismatches would arise.